nature chemical biology

Article

https://doi.org/10.1038/s41589-025-01885-5

Temporal oscillation of phospholipids promotes metabolic efficiency

Received: 11 September 2024

Accepted: 13 March 2025

Published online: 14 April 2025

Check for updates

Sen Yang[1,4], Yuan Wang[1,4], Sisi Huang[1], Tong Zhang[1], Pinglong Xu[1], Chao Jiang[1] & Cunqi Ye[1,2,3]

Biological timing is a fundamental aspect of life, facilitating efficient resource use and adaptation to environmental changes. In this study, we unveil robust temporal oscillations in phospholipid abundance as a function of the yeast metabolic cycle (YMC). These fluctuations, occurring throughout the cell division cycle, demonstrate a systematic segregation of various phospholipid species over time. Such segregation corresponds logically with their physical properties, generating entropic forces for membrane dynamics and biogenesis. Within the YMC, the temporal oscillations in phosphatidylethanolamine and phosphatidylcholine levels require biosynthesis from triacylglycerol as a crucial lipid reservoir, with phosphatidylinositol and phosphatidylserine synthesized primarily de novo. The orchestrated regulation of gene expression in biosynthesis pathways ensures precise temporal control of phospholipid dynamics, ultimately promoting metabolic efficiency.

Phospholipids play a fundamental role in life by facilitating biomembrane formation and intracellular signaling[1,2]. These amphiphilic molecules exhibit remarkable molecular diversity, characterized by a variety of polar head groups and aliphatic chains differing in length and degree of unsaturation[3]. In eukaryotic cells, phosphatidylcholine (PC), phosphatidylethanolamine (PE) and phosphatidylinositol (PI) are the most abundant phospholipids, with phosphatidic acid (PA), phosphatidylserine (PS), phosphatidylglycerol (PG) and cardiolipin present in lesser amounts[4]. While abundant lipids like PC and PE form the structural basis of membranes, the chemical and compositional diversity of phospholipids within the membrane environment substantially influences their biophysical properties and interactions with membrane-associated proteins[5–7]. Beyond their structural roles, signaling phospholipids, such as phosphoinositides generated through PI phosphorylation, are crucial for cellular signaling pathways, interacting with specific effector proteins to mediate diverse cellular responses[8,9].

During the cell division cycle, membrane dynamics, including expansion, remodeling and trafficking, necessitate tight coordination of lipid biosynthesis with various cellular regulatory mechanisms[10–15]. This coordination ensures the availability of sufficient membrane materials and proper signal transduction, orchestrating the successful progression of cell division and proliferation[16,17]. For example, in mammalian cells, fatty acid synthesis serves as a lipid checkpoint in the G1 phase, with insufficient synthesis suppressing lipid remodeling and entry into the S phase[17]. In yeast cells, translational control of lipogenic enzymes, such as acetyl-CoA decarboxylase, leads to oscillations in their protein abundance, with levels peaking late in the cell cycle[18–20]. This timing coincides with the accumulation of phospholipids and triglycerides, which also peak in abundance during this phase[13]. Despite these observations linking lipid metabolism to the eukaryotic cell cycle, the precise temporal dynamics of diverse phospholipid species production during cell division remain largely unknown.

A multitude of biosynthetic processes are temporally segregated to drive cell growth during the cell division cycle[12,21–26]. This temporal organization, regulated by an ultradian clock, establishes a metabolic hierarchy for optimizing energy efficiency, as exemplified by the yeast metabolic cycle (YMC)[26–28]. Within the YMC, both metabolites and transcripts oscillate in abundance[21,29–31], orchestrating a just-in-time mechanism to supply necessary components in a specific temporal sequence[32,33]. However, it remains unclear whether phospholipids

[1]Zhejiang Provincial Key Laboratory for Cancer Molecular Cell Biology, Life Sciences Institute, Zhejiang University, Hangzhou, China. [2]Department of Reproductive Endocrinology, Women's Hospital, Zhejiang University School of Medicine, Hangzhou, China. [3]Hainan Institute, Zhejiang University, Sanya, China. [4]These authors contributed equally: Sen Yang, Yuan Wang. e-mail: yecunqi@zju.edu.cn

exhibit temporal compartmentalization throughout the cell division cycle, and if so, the underlying logic and regulatory mechanisms remain unexplored. We employed the metabolic cycle established in the budding yeast *Saccharomyces cerevisiae* to investigate the temporal patterns of phospholipids. In this system, cell synchronization is achieved through high-density growth in an aerobic chemostat with a constant, continuous supply of limited nutrients[34]. Under these conditions, yeast cells undergo a robust ultradian rhythm in oxygen consumption while respiring the available glucose. This synchronization provides a unique opportunity to investigate the cell-intrinsic clock in the biosynthesis of phospholipids for membrane biogenesis under constant growth conditions.

Here we discovered temporal dynamics of phospholipid abundance in yeast cells undergoing the YMC, revealing periodic characteristics across their molecular diversity. Within a budding cycle, the phospholipids PE and PC exhibited opposing oscillations in abundance, independent of the composition of their fatty acyl chains. Unlike PE and PC, the abundance oscillations of PI and PS displayed temporal shifts depending on acyl unsaturation and length. Such temporal separation aligned consistently with their biophysical properties, influencing membrane states. Phospholipids promoting membrane disorders increased progressively at budding onset, followed by a rise in phospholipids stabilizing bilayers during bud growth. The timely regulation of rhythmic fluctuations in phospholipid abundance requires the programming of gene expression in biosynthesis, as well as triacylglycerol (TAG) serving as a lipid reservoir to support PE and PC synthesis. We propose that the oscillating phospholipid abundance throughout the cell division cycle represents a cell-intrinsic rhythm that facilitates cell-autonomous, thermodynamic control of biomembrane compositions for energy efficiency.

Results

Phospholipid levels oscillate during the YMC

We first established the YMC in a bioreactor using the prototrophic, haploid yeast strain CEN.PK (Fig. 1a). Following growth saturation at high density and subsequent starvation, robust cycles in oxygen consumption were induced by feeding with glucose-limited nutrients at a constant rate, while maintaining constant pH, temperature and aeration conditions[21]. Each cycle was about 4 h in length and characterized by distinct metabolic phases (oxidative (OX), reductive building (RB) and reductive charging (RC)) with an ordered progression (Fig. 1a)[21,35]. Next, we estimated the percentage of dividing cells during the YMC by microscopically counting budded cells and found that roughly 40% of the yeast population proceeded through the budding cycle during the YMC (Extended Data Fig. 1a), a proportion close to the approximately 50% observed using the diploid cells[21]. We developed a multiple reaction monitoring-based liquid chromatography–tandem mass spectrometry (LC–MS/MS) method capable of simultaneously detecting a library of 70 phospholipids common in yeast cells within a 25-min chromatographic run[36]. To ensure specific and sensitive quantification of phospholipids, we further optimized parameters for collision-induced fragmentation and validated their mass spectral-retention time for each phospholipid using yeast deletion mutants that disrupt phospholipid synthesis[36].

To elucidate changes in phospholipid abundance associated with cell division and growth within a budding cycle, we collected cell samples from two consecutive YMCs and conducted quantitative phospholipid analysis using the highly sensitive MS method after lipid extraction (Fig. 1a). Among the 70 molecular species of phospholipids quantified, we observed that the majority exhibited temporal oscillations in abundance within the YMC, which were consistent and repeatable in a subsequent cycle (Fig. 1b). Clustering analysis and a Sankey diagram revealed that the abundances of most PC and PI species peaked at similar times, during which the phospholipid PE exhibited reductions in abundance (Fig. 1b). Thus, the synchronized yeast cells in the YMC undergo periodic changes in phospholipid contents, varying across their molecular diversity.

To better correlate the oscillatory phospholipid abundance with their requirement for membrane biogenesis in cycling cells, we first adjusted the times of sampling points to the fractional times of a budding cycle (Fig. 1c). We designated the first OX phase point (t_6) as budding cycle 0 as the buds only appeared after the OX phase (Extended Data Fig. 1a). We next quantified factional levels of the abundant phospholipids PE, PC and PI and inspected their oscillation patterns. As illustrated in Fig. 1c, total PE abundance increased after the OX phase when the budding process began, coinciding with a decrease in total PC and PI abundance. Conversely, PE abundance began to decline as total PC and PI levels rose during the latter half of the budding cycle. Metabolic rate calculation further revealed a temporal order in the synthesis of abundant phospholipids in the cycling cells: transitioning from a dominant production of PE to a more active production of PC and PI throughout the budding cycle (Fig. 1d).

Periodic phospholipids vary in phase and amplitude

Given the robust oscillations observed in PE, PC and PI, we assumed that the oscillatory behavior of phospholipids follows a simple harmonic motion. This assumption simplifies the complex dynamics of phospholipid fluctuations, allowing for analytical tractability and clear predictions. Similar idealizations have been used to illustrate temporal dynamics under comparable conditions[28,37]. We thus applied the sine function to quantify the periodic characteristics of phospholipid abundance (Extended Data Fig. 1b; see Methods for details). Except for PS and PA, the abundances of PE, PC, PI, PG, lyso-PE (LPE) and lyso-PC (LPC) all displayed high confidence in sine periodicity (Fig. 1e,f). Specifically, the coefficient of determination (R^2) was recorded at 0.87 for PE and 0.88 for PC, denoting highly significant P values (1.3×10^{-9} for PE and 9.5×10^{-10} for PC; Fig. 1f and Supplementary Data 1). The phase shift in PE and PC resulted in alternating increases and decreases in abundance within budding cycles (Extended Data Fig. 1c), yielding an evident cyclic pattern in the PE-to-PC ratio (Extended Data Fig. 1d).

We calculated the time of the wave trough (T_{trough}) for each phospholipid class by adjusting it to the phase of a budding cycle (Fig. 1f,g). T_{trough} corresponds to the phase when the abundance reaches its lowest point (Extended Data Fig. 1b). Following this phase, the rate of synthesis exceeds consumption, persisting for half of the cycle duration. Our observations revealed that phospholipids that promote membrane curvatures, such as PE and LPC, exhibited their lowest abundances at the onset of budding (Fig. 1g). Although LPE is unlikely to exhibit lytic properties in membranes due to its cylindrical shape[38], its abundance change mirrors that of LPC, an inverted-conical lipid. This observation suggests that phospholipid acyl chain remodeling is active during the onset of budding, which may influence membrane properties, such as curvatures and dynamics. In contrast, phospholipids like PI, PC and PG, which contribute to bilayer formation, showed their lowest abundances around the second half of a budding cycle (Fig. 1g). For each phospholipid species, the amplitude is determined by the maximal difference between synthesis and consumption, represented by the peak-to-peak amplitude ($2A$; Fig. 1f). The abundant phospholipids like PE, PC and PI exhibited fluctuation magnitudes around 0.19, 0.12 and 0.11, respectively. Less abundant lipids, such as LPE and LPC, showed larger fluctuations around 0.80 and 0.46, respectively (Fig. 1f). The abundance variation in timing and magnitude among different phospholipid classes underscores the dynamic composition of phospholipid membranes throughout a budding cycle. Given the tight coupling between cell division and metabolic cycles under constant growth conditions with glucose-limited nutrients[21,25,31], yeast cells exhibited cell cycle-dependent alterations in phospholipid composition, with changes observed in the abundance of specific phospholipid head group types (Fig. 1h).

https://doi.org/10.1038/s41589-025-01885-5

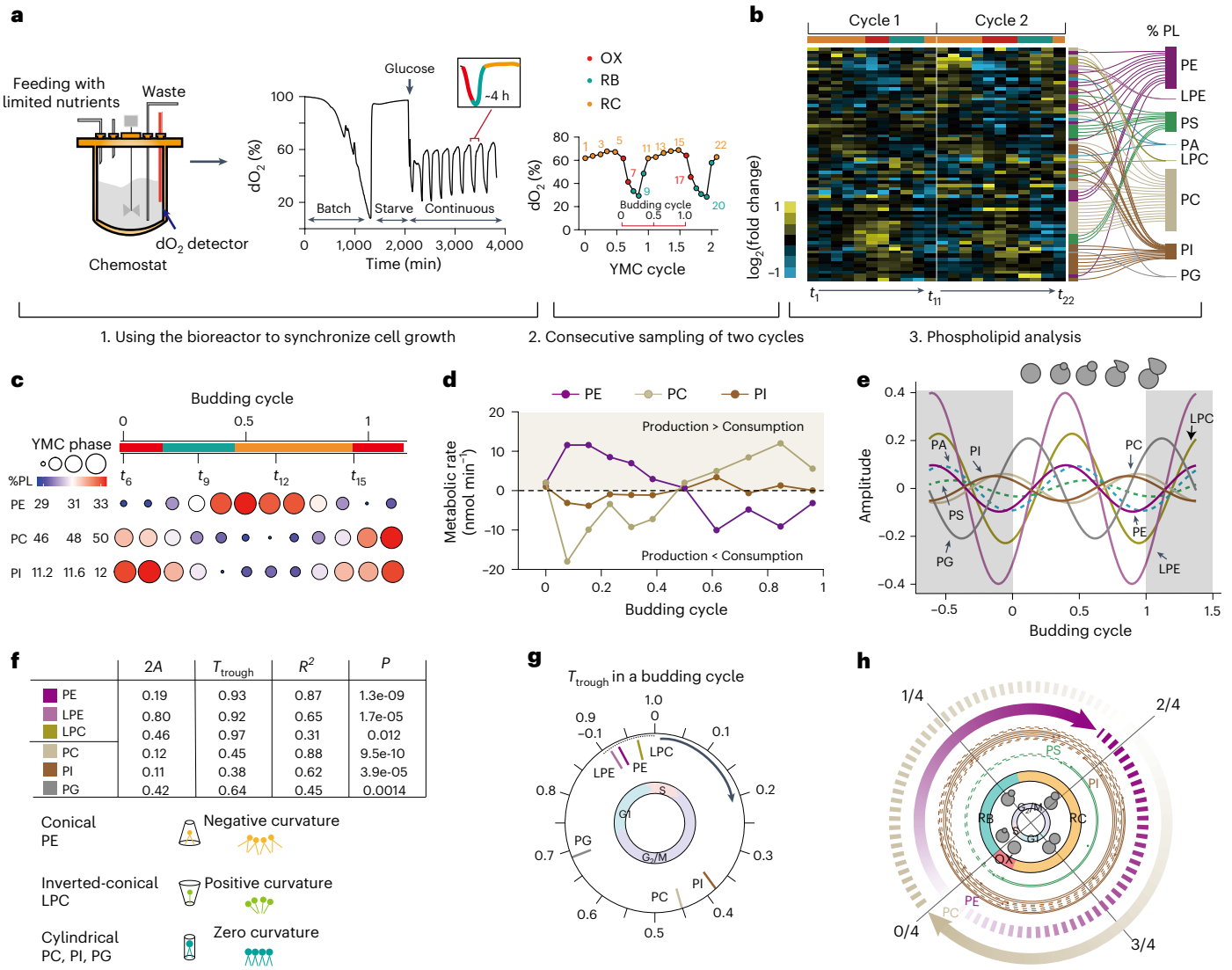

Fig. 1 | Phospholipids exhibit robust oscillations in abundance as a function of the YMC. a, Schematic of the continuous culture system (left) used to induce YMC oscillations, and sampling time points across two cycles (right). dO_2, dissolved oxygen (% saturation). **b**, Hierarchical clustering analysis of phospholipid abundances over the YMC. The Sankey diagram depicts the class-specific distribution of phospholipid species. **c**, PE, PC and PI abundance (% PL) during a yeast budding cycle, shown as bubble size and color gradient. **d**, PE, PC and PI metabolic rates during a budding cycle. Data represent average values from cells sampled over two cycles. Shading areas represent lipid production. **e**, Sine wave fitting of total abundance for major phospholipid classes. Solid lines indicate statistically significant fits ($P < 0.05$), while dashed lines represent nonsignificant fits. Shaded areas are used to highlight a budding cycle. **f**, Summary table of parameters with significant fitting. $2A$ refers to the maximum difference in phospholipid abundance, T_{trough} denotes the time corresponding to the lowest value of phospholipid abundance, R^2 indicates the adjusted coefficient of determination and P represents the statistical significance of curve fitting. **g**, Distribution of T_{trough} within a budding cycle for class-specific phospholipids. **h**, Schematic summary of phospholipid abundance oscillation across the YMC and cell cycle. Each line represents a specific phospholipid class with significant curve fitting ($P < 0.05$). For PI and PS, solid lines represent net phospholipid production, and dashed lines represent net phospholipid consumption. Gradient changes in line colors for PE and PC denote fluctuations in abundance. For PI and PS, subclass-specific abundances are grouped by acyl chain length and unsaturation. Statistical analyses were performed using a two-sided t-test in **e** and **f**.

Phospholipid oscillations vary by head group and acyl chain

To understand the potential impact of fatty acyl composition on phospholipid oscillations, we conducted tests to determine whether any individual phospholipid species displayed periodicity following a sine function. Among the 70 phospholipid species that we examined, 40 exhibited apparent sine periodicity ($P < 0.05$; Supplementary Data 2). Of note, we observed more significant fitting in abundant phospholipids (Extended Data Fig. 2). This bias could be partly attributed to the technical challenge of quantifying low-abundance phospholipids within a linear range, suggesting that the number of phospholipids exhibiting significant fitting may be underestimated.

Among all wave curves fitted with significance, individual species of PE and PC exhibited similarities to their total abundance wave curves, with minimal phase shifts (Fig. 2a,b). In contrast, PI and PS displayed distinct phase patterns within their respective species (Fig. 2c,d). While the total levels of PS did not show fitting significance, half of its species demonstrated robust sine periodicity (Fig. 2d). This finding suggests that, for a particular phospholipid class, its sine periodicity can be offset by species fluctuating in opposite directions.

We then examined the sine periodicity for each phospholipid class based on the total number of double bonds and acyl carbons. Consistent with the findings in individual PE and PC species, the abundances of PE

https://doi.org/10.1038/s41589-025-01885-5

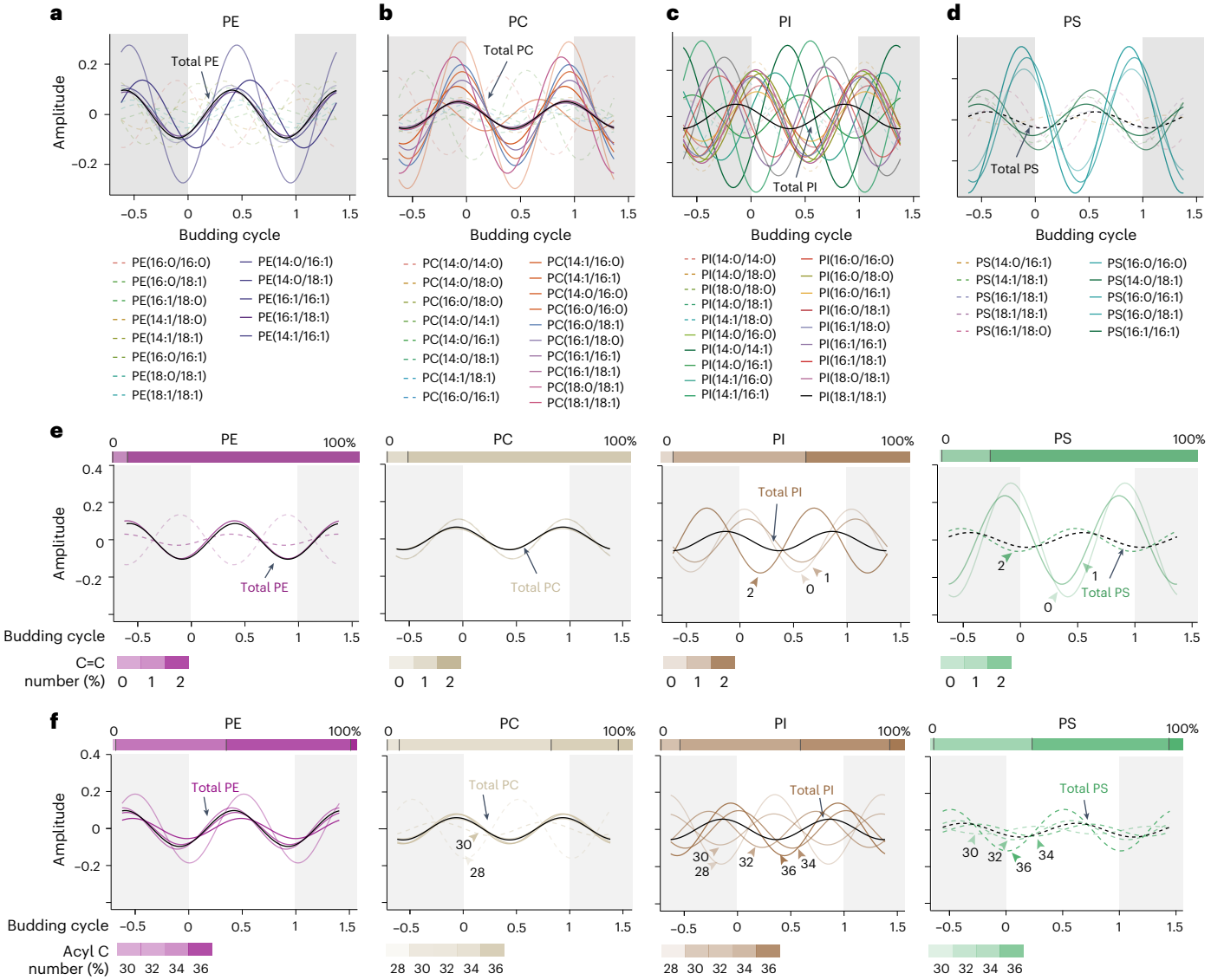

Fig. 2 | The periodic pattern of phospholipid abundance varies depending on the head group and acyl composition. a–**d**, Sine waves representing individual phospholipid species within specific classes, including PE (**a**), PC (**b**), PI (**c**) and PS (**d**). Curves in solid lines indicate fitting of statistical significance ($P < 0.05$), while dashed lines represent nonsignificant fitting. Please note that PE and PC exhibited minimal phase shifts within their molecular species, contrasting with PI and PS. **e**,**f**, Sine waves depicting major phospholipid classes characterized by their acyl composition in terms of the numbers of double bonds (**e**) and acyl chain carbons (**f**). Solid lines indicate fitting of statistical significance ($P < 0.05$), while dashed lines represent nonsignificant fitting. Please note that numbers represent the combined carbon atoms or double bonds in the fatty acid chains. Statistical analyses were performed using a two-sided *t* test in **a**–**f**. Shaded areas are used to highlight a budding cycle.

and PC subclasses grouped by double bond and acyl carbon numbers exhibited remarkably similar sine waves to the total PE and PC (Fig. 2e,f). However, for PI and PS, we observed that phospholipids with greater unsaturation (double bond number = 2) and shorter fatty acyl tails (carbon number = 28, 30) exhibited an earlier T_{trough} compared to phospholipids with lower unsaturation (double bond number = 0, 1) and longer tails (carbon number = 32, 34, 36; Fig. 2e,f). Therefore, the composition of acyl chains in PI and PS partitioned their species into different wave phases. Similar to how head groups that influence membrane biophysical states shifted the wave phases of phospholipids, those with more unsaturated and shorter acyl tails in PI and PS, which tend to promote membrane disorders, showed a gradual increase in abundance around budding onset, preceding those with less unsaturation and longer acyl tails.

TAG bursts support the synthesis of PC and PE during the YMC

As the neutral lipid TAG serves to provide reservoirs for membrane formation, we sought to investigate whether its abundance also undergoes cyclic changes during the YMC. We analyzed 68 common TAG species in yeast cells collected from two consecutive YMCs using a highly sensitive LC–MS method (Fig. 3a). We observed sharp spikes in almost all TAG species just before the onset of budding, followed by a gradual decrease throughout the cycle (Fig. 3a). Unlike the oscillations seen in phospholipid levels throughout the budding cycle, the synchronous tapering pattern of TAG content following a burst was unaffected by the acyl composition of unsaturation and length (Fig. 3a,b). Moreover, most genes involved in TAG synthesis exhibited their peak expression during the RC phase, aligning with the timing before budding[31] (Extended Data Fig. 3a,b). This predicts a metabolic outcome that TAG synthesis is suppressed during bud growth. Indeed, TAG synthesis only markedly exceeded consumption right before bud emergence (Fig. 3c). In particular, TAG consumption was most pronounced during the 0.4–0.8 phase of the budding cycle (Fig. 3c), coinciding with the progressive increase in PC and PI levels.

https://doi.org/10.1038/s41589-025-01885-5

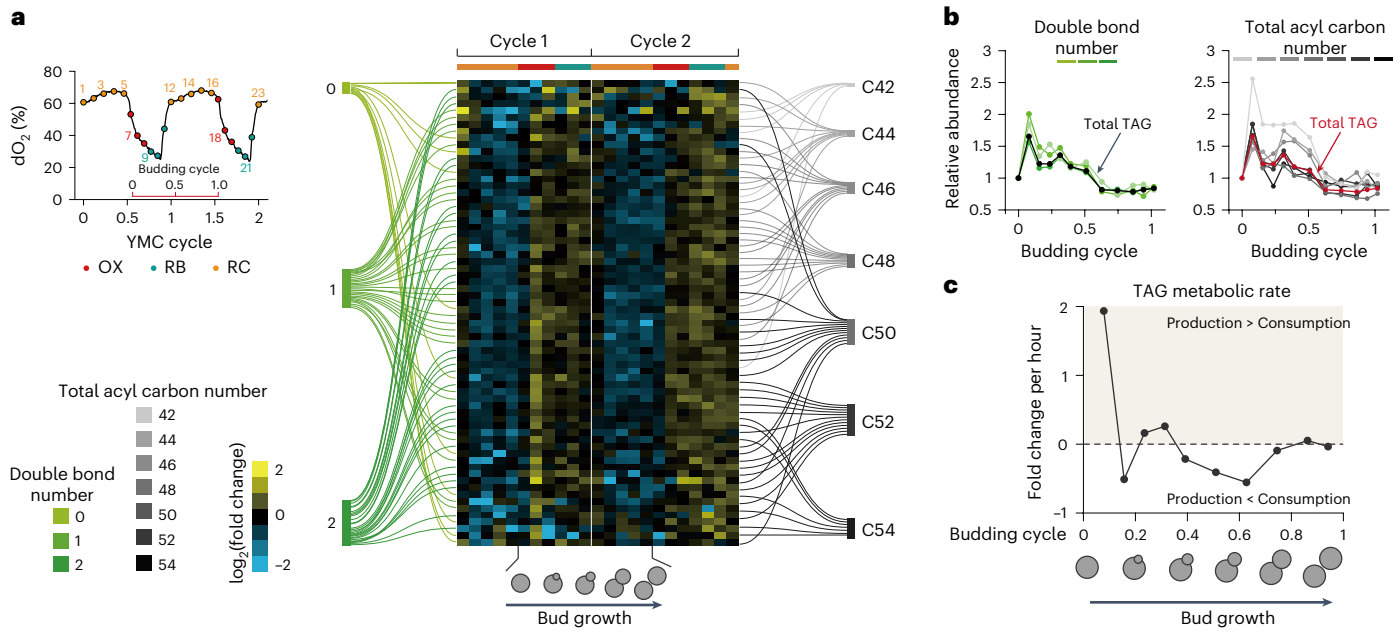

Fig. 3 | TAG abundance fluctuates in a burst-and-taper mode during the YMC. **a**, Heatmap illustrating TAG abundance throughout two consecutive YMCs. Sample collection times and corresponding budding phases are indicated. The Sankey diagram denotes TAG species with different degrees of unsaturation (left) and acyl chain length (right). **b**, Dynamic abundances of total TAG and TAGs in subgroups with indicated numbers of double bonds and acyl chain carbons in a budding cycle. **c**, TAG metabolic rates within a budding cycle. Shading areas represent lipid production. Data represent average values from cells sampled over two cycles.

To further understand the relationship between TAG dynamics and phospholipid metabolism, we investigated the turnover of glycerolipids within the YMC by feeding isotopic [U–^{13}C6] glucose. To minimize perturbations to the abrupt burst of respiration in the OX phase, we opted to infuse the isotopic glucose medium during the early RC phase, with cycling cells approaching the completion of the first half of a budding cycle (Fig. 4a). While glucose-derived ^{13}C gradually diluted the pool of nonlabeled carbon metabolites, we observed a substantial decrease of approximately 25% and 50% in unlabeled TAG within 100 and 200 min of infusion, respectively (Fig. 4b). This dynamic turnover reveals active use of the TAG pool, likely for phospholipid synthesis. Interestingly, despite the infusion occurring when PC levels were steadily increasing, we did not observe an immediate decrease in PC levels within the initial 100 min infusion of [U–^{13}C6] glucose (Fig. 4c). However, there was a moderate decrease of approximately 25% in PC within 200 min (Fig. 4c). This delayed turnover of PC suggests that unlabeled TAG may have provided lipid backbones for PC synthesis. The delayed turnover of PE was expected (Fig. 4c), as PE levels began to steadily increase around the onset of budding, approximately 120 min after infusion. In contrast, PS and PI exhibited decreases in their unlabeled levels within 100 min, continuing to reduce to less than 50% within 200 min (Fig. 4c). This suggests that PS and PI might be preferentially synthesized de novo.

However, our attempts to detect the newly synthesized phospholipids with fully ^{13}C labeling were unsuccessful due to the slow dilution rate of glucose within the YMC. To overcome this limitation, we performed a batch culture switch for a rapid exchange of isotopic carbon. Cells were precultured in [U–^{13}C6] glucose medium until saturation to synchronize them in the quiescence (G0) phase, mimicking the YMC condition[39], and then switched to regular medium containing nonlabeled glucose (Fig. 4d). These cells underwent two rounds of doubling before quantitative lipid analysis (Fig. 4d). This switch condition facilitated deprivation of cellular ^{13}C, as evidenced by an increase in fully ^{12}C-labeled TAG and a decrease in fully ^{13}C-labeled TAG after the two rounds of doubling (Fig. 4e). Both unlabeled and labeled TAG levels decreased substantially as expected in the lipodystrophy mutant *pah1Δ* (Fig. 4e).

When a phospholipid is synthesized fully de novo, approximately 50% of its newly synthesized amount would consist of the fully ^{12}C-labeled form after one round of doubling in regular glucose medium. Consistent with this prediction, unlabeled PI and PS accounted for 50% of their total content after one round of doubling (Fig. 4f), suggesting that PI and PS are preferentially synthesized de novo. After two rounds of doubling, PS became fully replaced by its unlabeled counterparts, while a portion of labeled PI remained (Fig. 4f). This halt in the turnover of PI may be due to the recycling of labeled inositol groups.

In stark contrast, PC fully labeled with ^{12}C was barely detectable after one round of doubling and increased to only 20% after two rounds (Fig. 4f). Similarly, fully ^{12}C-labeled PE only reached 15% and 60% after one and two rounds of doubling, respectively (Fig. 4f). Such fully ^{12}C-labeled PE might be attributed to the decarboxylation of PS, which serves as a major route for PE biosynthesis (Fig. 4g). The disparate labeling dynamics observed for PC and PE compared to PI and PS suggest that the synthesis of PC and PE might mainly rely on the deposited ^{13}C-TAG, rather than undergoing a de novo process using ^{12}C derived from glucose (Fig. 4g). Importantly, the relatively slow incorporation of ^{12}C in PC and PE was not due to unequal turnover of their head groups choline and ethanolamine (Extended Data Fig. 3c). In the *pah1Δ* mutant, where TAG synthesis is restricted, there was a substantial elevation of newly synthesized PC and PE with fully labeled ^{12}C (Fig. 4f). This indicates that the synthesis of PE and PC was compelled to follow the de novo synthesis route under TAG deficiency. Taken together, these findings suggest that TAG serves as a fuel source for the production of PC and PE within the YMC, with a preferential supply of PC.

TAG biosynthesis is essential for PE and PC oscillations

To investigate whether TAG biosynthesis is required for PE and PC oscillations, we constructed the *dga1Δlro1Δ* mutant, which blocks TAG biosynthesis, and further assessed its ability to perform metabolic cycles.

https://doi.org/10.1038/s41589-025-01885-5

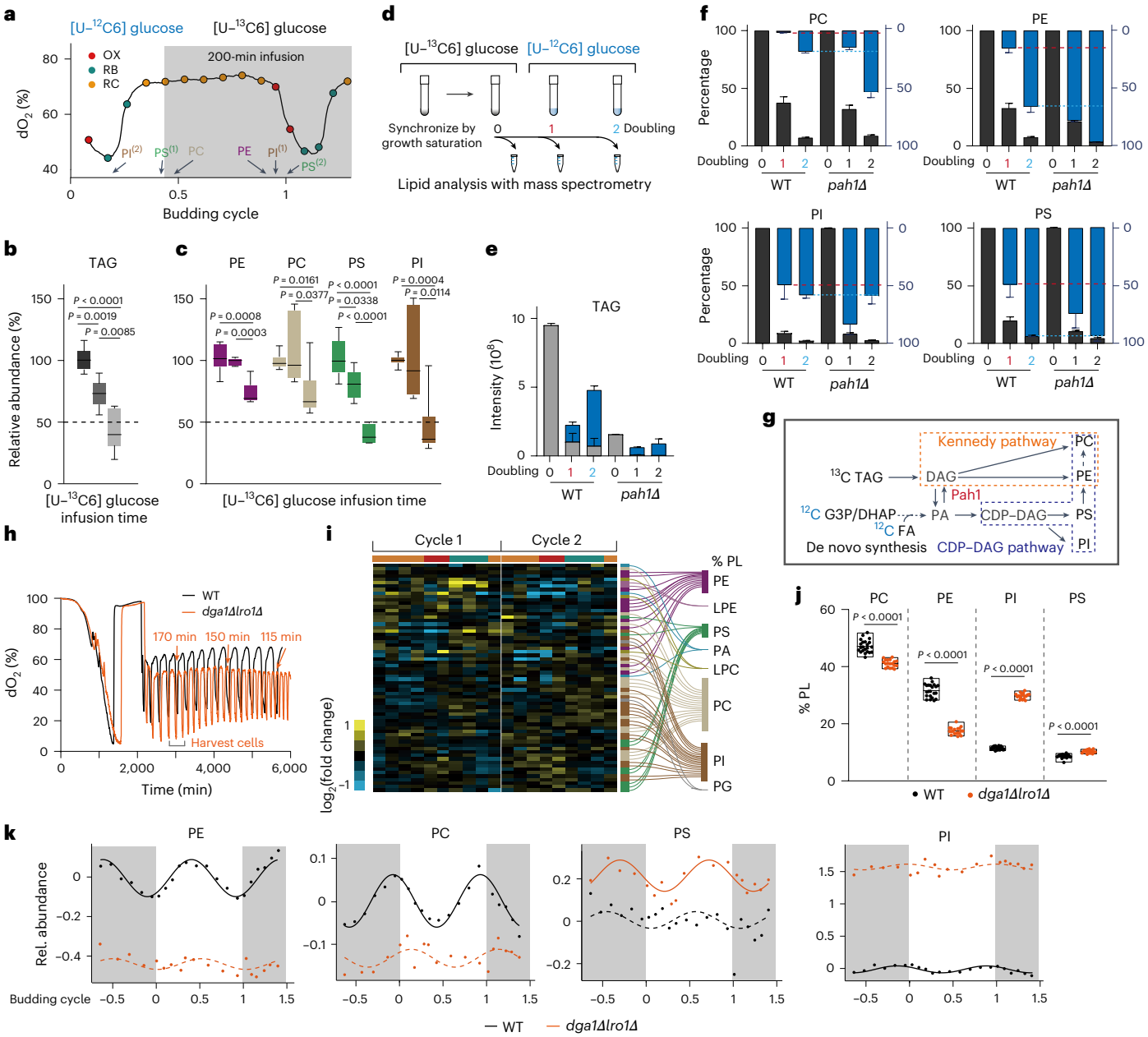

Fig. 4 | TAG fuels temporal oscillations in PE and PC production. a, [U–^{13}C6] glucose isotopic tracing schematic. YMC cells (RC phase) switched to labeled medium for 200 min (shading areas); samples collected every 20 min (colored dots). Phospholipid T_{trough} times are shown. PI/PS subclass double bond numbers in parentheses. **b**,**c**, TAG (**b**) and phospholipid (**c**) relative abundance before and after [U–^{13}C6] glucose infusion. Data normalized to pre-infusion levels ($n = 6$ biologically independent samples). Postinfusion data grouped into 0–100 min ($n = 5$ biologically independent samples) and 100–200 min ($n = 6$ biologically independent samples). Mean ± s.d. **d**, RIL schematic for quantifying phospholipid and TAG turnover/synthesis. Cells were fully labeled with [U–^{13}C6] glucose, then switched to unlabeled medium for two doublings. **e**, ^{13}C (gray) and ^{12}C (blue) TAG abundance in WT and *pah1Δ* cells before and after two doublings ($n = 3$ biologically independent samples). Mean ± s.d. **f**, Phospholipid turnover and synthesis, measured by RIL. Data (% of full ^{13}C labeling) normalized to preswitch levels ($n = 3$ biologically independent samples). Mean ± s.d. **g**, Phospholipid biosynthesis in *S. cerevisiae*. **h**, Oxygen consumption curves of WT and *dga1Δlro1Δ* cells. **i**, Hierarchical clustering of phospholipids in *dga1Δlro1Δ* cells across the YMC. Sankey diagram shows class distribution. **j**, PE, PC, PI and PS abundance (% PL) across the YMC ($n = 22$ for WT, $n = 19$ for *dga1Δlro1Δ*, biologically independent samples). **k**, PE, PC, PS and PI abundance in WT and *dga1Δlro1Δ* cells over the YMC. Solid lines, significant fit ($P < 0.05$); dashed lines, nonsignificant. Box plots (**b**, **c** and **j**), interquartile range, mean and min/max. whiskers. (**b**-**c**,**j**) Unpaired t-test; (**k**) two-sided *t* test. Shaded areas are used to highlight a budding cycle. RIL, reverse stable isotope labeling.

Without TAG biosynthesis, the mutant cells displayed unstable cycles in oxygen consumption, with cycling times continuously decreasing (Fig. 4h). Quantitative analysis of phospholipids in *dga1Δlro1Δ* cells from two consecutive cycles revealed that the obvious temporal compartmentalization of phospholipids across their molecular diversity observed in WT cells was disrupted by *dga1Δlro1Δ* (Fig. 4i). In particular, cycling cells lacking *DAG1* and *LRO1* exhibited reductions in total PC and PE levels and pronounced elevations in total PI levels (Fig. 4j). Interestingly, while PS exhibited sine periodicity within the YMC, the robust oscillations of PC and PE, including those observed with the respected classifications of their acyl compositions, were disrupted in the mutant (Fig. 4k, Extended Data Fig. 3d and Supplementary Data 3). These findings are consistent with the role of TAG serving to provide reservoirs for the timely production of PC and PE,

https://doi.org/10.1038/s41589-025-01885-5

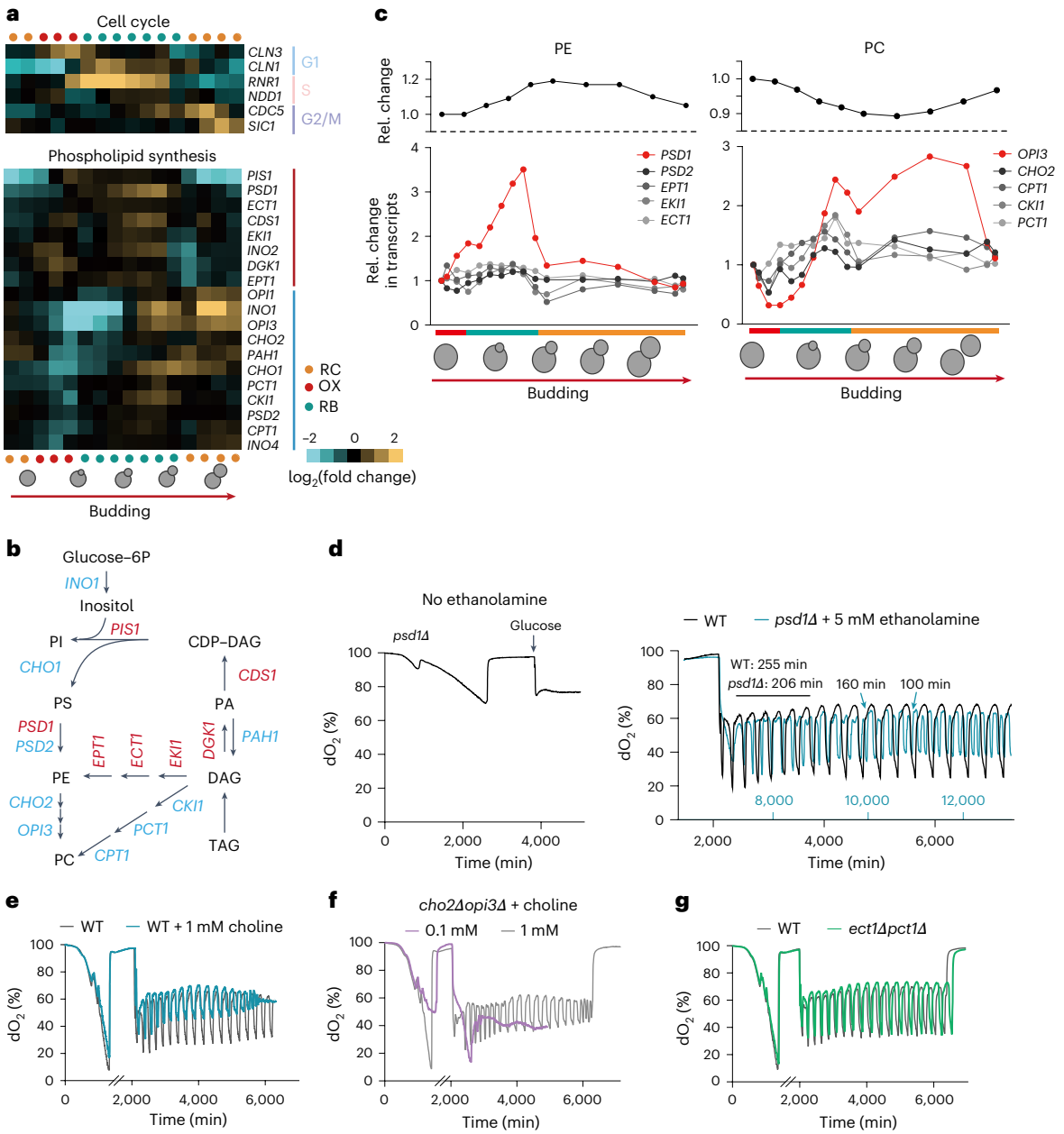

Fig. 5 | Oscillatory transcriptional control of the PS–PE–PC metabolic axis sustains the YMC. a, Heatmap illustrating the oscillatory expression of genes involved in cell cycle (top) and phospholipid biosynthesis (bottom) across the YMC. The heatmap is generated using RNA-seq data previously published[31]. **b**, Schematic of the phospholipid biosynthetic pathway in *S. cerevisiae* highlighting key genes. Genes associated with PC and PE biosynthesis are highlighted in red and blue, respectively, to emphasize their temporal segregation at the transcriptional level. **c**, Temporal oscillations in the abundance of PE and PC and in the transcript levels of their respective biosynthetic genes within a budding cycle. **d**, Left, the oxygen consumption curve of *psd1Δ* cells; right, oxygen consumption curves of WT and *psd1Δ* mutants with supplemented with 5 mM ethanolamine. **e**, Oxygen consumption curves of WT cells with or without 1 mM choline. **f**, Oxygen consumption curves of *cho2Δopi3Δ* mutants supplemented with 0.1 mM and 1 mM choline. **g**, Oxygen consumption curves of WT and *ect1Δpct1Δ* cells.

whose deficiency disrupts their oscillatory patterns as well as efficient, sustainable YMCs.

Transcriptional control of the PS–PE–PC axis sustains YMC

Given the pervasively periodic gene expression during the YMC, we sought to determine whether the temporal dynamics of phospholipid abundance were an outcome of oscillatory transcriptional regulation. Analyzing a previously published transcriptome dataset[31], we observed temporal variation in transcript abundance for genes involved in phospholipid synthesis, with peak timing spanning the YMC (Fig. 5a). This periodic pattern closely correlates with the temporal expression profiles of many genes involved in the cell cycle, such as *CLN1* and *CLN3* (G1 phase), *RNR1* and *NDD1* (S phase) and *CDC5* and *SIC1* (G2/M phase; Fig. 5a), suggesting that transcriptional regulation of phospholipid synthesis is linked to cell cycle progression in these cycling cells. In particular, genes in two major pathways for PE biosynthesis (Fig. 5b), including *PSD1* in the pathway of mitochondrial PS decarboxylation and *EKI1*, *ECT1* and *EPT1* in the PE branch of the Kennedy pathway, peaked around the onset of budding (Fig. 5c). In contrast, genes involved in PC synthesis (Fig. 5b), such as *CHO2* and *OPI3* in PE methylation, and *CKI1*, *PCT1* and *CPT1* in the PC branch of the Kennedy pathway, exhibited peak expression levels in the latter half of the budding cycle (Fig. 5c).

https://doi.org/10.1038/s41589-025-01885-5

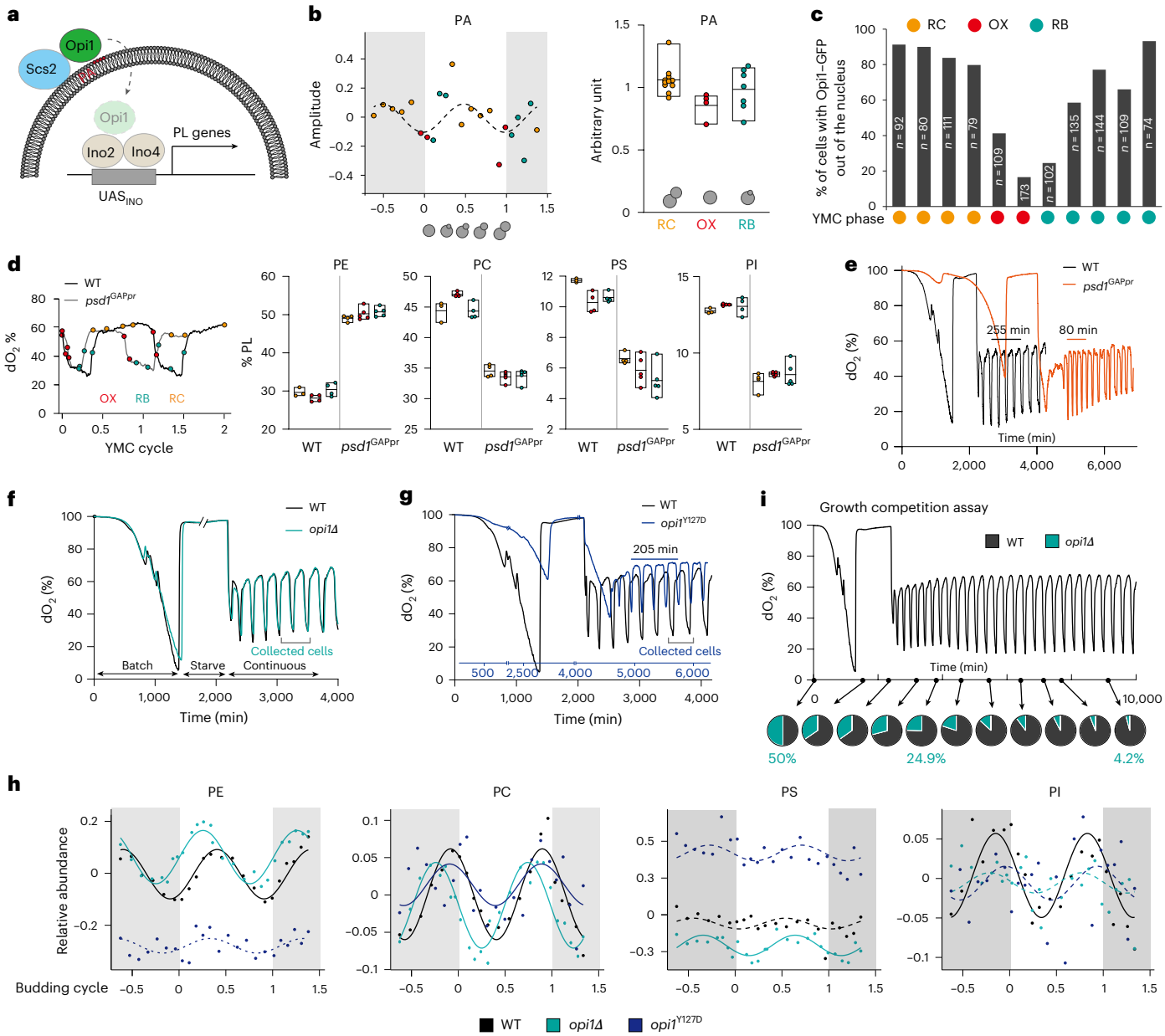

Fig. 6 | Disruption of the Henry regulatory circuit shifts temporal oscillations in phospholipids, compromising competitive growth during the YMC. **a**, Schematic of the Henry regulatory circuit. **b**, Left, relative abundance of PA in WT cells at indicated budding phases across two consecutive cycles, depicted with a fitting curve that is not statistically significant; right, relative changes in PA levels in WT cells collected at indicated phases (RC/OX/RB, $n = 11/4/7$ biologically independent samples). **c**, Quantitative analysis of the percentage of cells with Opi1–GFP signals outside the nucleus during the YMC. The number (n) indicates the cells counted for quantification. **d**, Relative phospholipid levels in WT and the *psd1*^{GAPpr} mutant of constitutive *PSD1* expression. Samples collected at indicated phases ($n = 3/4/4$ biologically independent samples in RC/OX/RB of WT; $n = 4/5/5$ biologically independent samples in RC/OX/RB of *psd1*^{GAPpr}). **e**, Oxygen consumption curves of WT and the *psd1*^{GAPpr} mutant. **f**, Oxygen consumption curves of WT and the *opi1Δ* mutant. **g**, Oxygen consumption curves of WT and the *opi1*^{Y127D} mutant. **h**, Relative abundance of PE, PC, PS and PI in WT, *opi1Δ* and *opi1*^{Y127D} cells over the YMC, depicted with fitting curves. Solid lines indicate fitting of statistical significance ($P < 0.05$), while dashed lines represent nonsignificant fitting. **i**, Growth competition between WT and *opi1Δ* cells (equal initial proportions). Box plots (**b**,**d**), interquartile range, mean, min/max whiskers. **h**, Two-sided t-test. Shaded areas are used to highlight a budding cycle.

The active expression windows for genes in PE and PC biosynthesis aligned temporally before their abundance peak (Fig. 5c). Notably, among these dynamically expressed genes, *PSD1* and *OPI3* exhibited the highest amplitudes, suggesting that their respective pathways, PS decarboxylation for PE synthesis and PE methylation for PC synthesis, play crucial roles in controlling the temporal oscillations of PE and PC abundance.

Blocking Psd1-mediated PE synthesis abolished the YMC (Fig. 5d). Even in the presence of exogenous ethanolamine, the *psd1Δ* mutant exhibited unstable cycles with shortened cycling times and reduced oxygen consumption (Fig. 5d). Similarly, exogenous choline, which redirects PC synthesis from PE methylation to the Kennedy pathway[40], disrupted the synchrony of the YMC in WT cells (Fig. 5e). Without the PE methylation pathway for PC synthesis, exogenous choline failed to sustain stable metabolic cycles in the mutant cells (Fig. 5f). In contrast, blocking the Kennedy pathway by *ect1Δpct1Δ* had negligible effects on the YMC (Fig. 5g). These findings collectively highlight the essential role of the PS–PE–PC metabolic axis in regulating the temporal

oscillation of PE and PC abundance, likely crucial for the coordinated, efficient cycling of metabolism within the YMC. Given that TAG synthesis is crucial for YMC progression and serves as a main provider for PC synthesis (Fig. 4f, g), these findings also suggest that in cycling cells, TAG likely fuels PC synthesis primarily through a coordinated pathway involving the TAG–DAG–PA axis and the PS–PE–PC axis, rather than solely relying on the DAG-dependent Kennedy pathway.

Unlike the synchronous oscillation observed in the expression of genes involved in PE and PC synthesis, the transcriptional regulation of PI synthesis exhibits segregation. Specifically, the expression timing of *PIS1*, encoding PI synthase, and *INO1*, encoding the rate-limiting enzyme for generating the *myo*-inositol precursor, differed within a budding cycle (Extended Data Fig. 4a). Interestingly, the *ino1Δ* mutant showed stable metabolic cycles with *myo*-inositol supplementation, albeit with a mild reduction in oxygen consumption (Extended Data Fig. 4b). Therefore, the transcriptional regulation of PI synthesis appears dispensable for sustaining the YMC.

Henry circuit drives lipid cycling for optimal YMC growth

We next investigated the activity of the Henry regulatory circuit within the YMC, a transcriptional program controlling phospholipid synthesis in response to the abundance of the phospholipid precursor PA (Fig. 6a). During the OX phase before budding, PA reached its lowest abundance (Fig. 6b). In line with PA depletion triggering the release of Opi1 from the endoplasmic reticulum (ER) for nuclear translocation[41], Opi1–GFP transiently appeared in the nucleus around budding onset (Fig. 6c and Extended Data Fig. 5a). During this period, nuclear Opi1 led to the transcriptional repression of genes in PC biosynthesis (Fig. 5c).

Surprisingly, genes required for PE biosynthesis, such as *PSD1* and *EPT1*, were transcriptionally repressed before Opi1 nuclear translocation and derepressed even when Opi1 was in the nucleus (Fig. 5c). This unexpected finding contradicted the expected coregulation of both PC and PE biosynthetic genes under the Henry regulatory circuit, as they contain *cis*-acting inositol-sensitive upstream activation sequences (UAS_{INO}). However, the deletion of *OPI1* led to substantial increases in mRNA levels of these UAS_{INO} genes in YMC cells, including the PE biosynthetic genes *PSD1* and *EPT1* (Extended Data Fig. 5b), confirming their regulation under the Henry regulatory circuit. We speculated that variation in the composition of the UAS_{INO}-containing promoter might subtly tune expression timing, resulting in a phase shift in phospholipid oscillation. To test this hypothesis, we disrupted *PSD1* regulation from the Henry regulatory circuit by constitutively expressing an additional copy of *PSD1* from the HO locus ($psd1^{GAPpr}$). This expression of *PSD1* led to elevated PE levels and reductions in PC, PS and PI levels (Fig. 6d), underlying an aberrant upregulation of Psd1-mediated decarboxylation for PE production. This caused severe growth delay under batch conditions, defective oxygen consumption and shortened cycling times under YMC conditions (Fig. 6e). These findings further substantiate that the transcript periodicity of *PSD1* is crucial for maintaining phospholipid composition throughout the budding cycle, contributing to sustaining metabolic cycles.

To further elucidate the impact of the Henry regulatory circuit on phospholipid oscillations within the YMC, we next used two mutants, *opi1Δ* and $opi1^{Y127D}$, to constitutively activate and repress phospholipid synthesis, respectively[42]. While *opi1Δ* exhibited growth indistinguishable from WT under both batch and YMC conditions (Fig. 6f), $opi1^{Y127D}$ showed reduced oxygen consumption, retarded batch growth and shortened cycling times of the YMC (Fig. 6g). The transcriptional activation of phospholipid synthesis by *opi1Δ* resulted in moderate increases in PE levels and decreases in PS levels (Fig. 6c,h). These changes resembled the effects observed upon constitutive expression of *PSD1*, albeit to a lesser extent. This suggests that PS decarboxylation is a major effector pathway in the YMC governed by the Henry regulatory circuit. Consistently, the transcriptional repression of phospholipid synthesis by $opi1^{Y127D}$ led to a marked reduction in PE levels and a corresponding increase in PS levels, accompanied by the loss of sine periodicity in PI (Fig. 6h).

Notably, the abundance of phospholipids in the *opi1Δ* mutant remained temporally segregated within the YMC (Extended Data Fig. 5d), with evident phase shifts observed in PE, PC and various PI and PS species (Fig. 6h, Extended Data Fig. 5e–g and Supplementary Data 1 and 4), while its cyclic growth was unaffected (Fig. 6f). This indicates that temporally controlling phospholipid abundance is not essential for sustaining the YMC. However, considering the energetic efficiency of temporal compartmentalization of metabolism within the YMC, we reasoned whether the competitive growth of the *opi1Δ* mutant might be compromised. To test this, we performed a growth competition experiment by coculturing WT and *opi1Δ* cells starting at the same proportion. With the progression of the YMC, *opi1Δ* mutant cells were gradually outcompeted by WT cells (Fig. 6i). This confirms the growth advantage under the Henry regulatory circuit, suggesting that the autonomous, temporal oscillation of phospholipids promotes metabolic efficiency during the YMC.

Discussion

The synthesis of lipid bilayers demands substantial energy, often representing the most significant portion of cellular energy expenditure[43]. This high cost necessitates energy efficiency in lipid synthesis across various timescales. However, cellular phospholipids encompass a vast array of molecular species, exhibiting chemical diversity in their structure and compositional diversity in biomembranes. This molecular diversity operates at multiple levels, including organism, cell type, organelle, bilayer–leaflet and membrane subdomain, presenting a substantial challenge in understanding the temporal processes involved in establishing functional phospholipid membranes. In light of this complexity, our study revealed a fascinating temporal compartmentalization of phospholipids across different molecular species during yeast budding cycles. Unlike many previous studies that provide static snapshots of lipid profiles[10,44], we employed a chemostat system to synchronize yeast cell growth and collected samples at defined time points. By integrating a robust, high-sensitivity LC–MS/MS-based approach capable of comprehensively analyzing 70 common yeast phospholipids[36], we uncovered high-resolution temporal oscillations throughout the cell division cycle. These oscillations were characterized by phospholipid class-specific and species-specific variations in phase shift and dynamic amplitude. However, we acknowledge the technical challenge posed by the presence of nondividing cells within the synchronized yeast population. While their influence on lipid changes, particularly fluctuation magnitudes, cannot be ignored, it is plausible that these fluctuations, particularly temporal patterns, are largely independent of the nondividing cell population due to their lack of need for membrane biogenesis.

The temporal oscillation of phospholipids is closely correlated with their biophysical properties, as illustrated in Fig. 1f,h. Conical phospholipids like PE and inverted-conical phospholipids like LPC possess unique biophysical properties that generate membrane curvatures[45]. Their increases at the onset of budding likely enhance entropic force to facilitate membrane deformation by disrupting bilayer membranes[46–48], necessitating membrane dynamics as an energetically favorable strategy. In contrast, bilayer-forming phospholipids such as PC and PI begin to increase as the cycle is about halfway complete, which may be thermodynamically favored to stabilize the formation of bilayer membranes[49]. This temporal segregation based on lipid polymorphism unveils a biophysical logic underlying cell-autonomous, thermodynamic control for membrane biogenesis throughout the cell division cycle. We proposed that the opposing oscillations in PE and PC have a crucial role in shaping the overall membrane biophysics, while fine-tuning is achieved through fluctuations in PI and PS, with varying acyl compositions at specific membrane domains. Specifically, phospholipid compositions may promote a more fluid membrane during

the early stage of the budding cycle, facilitating membrane expansion and vesicle trafficking. In the latter half of the cycle, the membrane may transition to a less fluid state, potentially creating a more stable membranous environment conducive to the growth of the cell and its organelles. However, how these lipid changes specifically alter the physical properties of different membrane systems, such as the plasma membrane, mitochondrial membranes and vacuolar membranes, remains to be elucidated. Further investigations into lipid changes within specific organelles and their coordinated transport during the cell cycle will be crucial to fully understand the functional significance of these dynamic changes in lipid composition.

While PE methylation and the Kennedy pathway for PC synthesis exhibit acyl chain preferences[50,51], the oscillation patterns of individual PE and PC species closely mirror their respective total abundances in cells undergoing the YMC. These findings suggest that acyl chain specificity may not be a critical determinant of PE and PC synthesis for cell cycle progression. Interestingly, the composition of acyl chains in PI species partitions them into distinct wave phases. We speculate that this oscillation pattern may be linked to organelle-specific PI distribution and the temporal biosynthesis of phosphoinositides, which play diverse signaling roles in the Golgi, plasma membrane and endosomes[8,52,53]. Furthermore, PS decarboxylation exhibits a preference for forming di-unsaturated PE, potentially due to the mitochondrion-dependent selective import of such di-unsaturated PS species[54,55]. Our observation that the oscillation pattern of di-unsaturated PS temporally aligns with that of PE in cycling cells suggests that di-unsaturated PS may serve as a precursor for PE synthesis.

The precise control of temporal oscillations of phospholipids relies on the following two key mechanisms: TAG synthesis and a transcription program governing phospholipid synthesis. In our study, we found that TAG serves as a major precursor for PC and PE synthesis, while PS and PI are primarily synthesized de novo. PC and PE synthesis occurs via the following two major pathways: the Kennedy pathway and the CDP–DAG pathway[4,5,56] (Fig. 4g). In the Kennedy pathway, DAG condenses with activated polar head groups (CDP-choline and CDP-ethanolamine). In the CDP–DAG pathway, PA, after activation to CDP–DAG, reacts with serine to produce PS, which can be subsequently decarboxylated to PE in the mitochondria and methylated to produce PC in the ER. While both DAG and PA can be derived from TAG, PA can also be synthesized de novo through the acylation of glycerol-3-phosphate and dihydroxyacetone phosphate[5,56]. The finding that blocking the Kennedy pathway had a negligible effect on the YMC suggests that this pathway may not be a major contributor to PE and PC synthesis, or that the CDP–DAG pathway can compensate effectively under these conditions. In contrast, we found that the oscillatory transcriptional control of the PS–PE–PC metabolic axis, downstream of the CDP–DAG pathway, is required for PE and PC abundance oscillation and YMC progression. It is likely that in these cycling cells, TAG-derived PA undergoes activation to synthesize PS, and subsequently, the TAG-derived PS, rather than the DAG-dependent Kennedy pathway, fuels the synthesis of PE and PC via the PS–PE–PC metabolic axis. We speculate that PS synthesized from PA, derived from different sources, may be differentially trafficked to the mitochondria and the plasma membrane. This source-based segregation of lipid precursors—whether from TAG or de novo synthesis—may be subject to distinct regulatory controls to meet the specific membrane requirements of different cellular compartments, potentially related to the timing and biomass production needed during the cell cycle.

In further support of this idea, we observed that the transcriptional oscillations of *PSD1* and *OPI3*—genes involved in PS decarboxylation for PE synthesis and PE methylation for PC production—exhibit the most pronounced periodic patterns among all phospholipid biosynthetic genes. This finding highlights the critical role of the transcriptional regulation of PS decarboxylation and PE methylation in the oscillation of phospholipid abundance during the YMC. We also note that additional regulatory mechanisms beyond Opi1-mediated repression likely influence the timing of *PSD1* expression. Variations in UAS_{INO}-containing promoters, or the presence of other regulatory motifs, may impact the recruitment of chromatin remodeling complexes, leading to changes in chromatin accessibility that influence the timing of gene expression. Additionally, factors such as transcript stability may contribute to the observed temporal regulation of *PSD1*. These observations raise important questions about the complexity of phospholipid gene regulation and highlight the need for further investigation into these additional regulatory pathways in the cell division cycle.

In summary, we propose that temporal oscillation of phospholipids throughout the cell division cycle represents an inherent cellular rhythm that allows the integration of environmental cues, such as nutrient quality and quantity, to regulate the timing of phospholipid synthesis, which ultimately modulates metabolic efficiency. A central aspect of our findings is the pivotal role of the PS–PE–PC axis in sustaining phospholipid oscillations, with the synthesis and turnover of PE at its core. This coordination occurs through processes such as mitochondrial PE biosynthesis, subsequent export to the ER and methylation, which collectively tune the PE-to-PC ratios. In this light, mitochondria may play a central role in this cellular rhythm, acting as a timekeeper for phospholipid synthesis and coordinating adjustments in membrane biophysics with bioenergetic states.

Online content

Any methods, additional references, Nature Portfolio reporting summaries, source data, extended data, supplementary information, acknowledgements, peer review information; details of author contributions and competing interests; and statements of data and code availability are available at https://doi.org/10.1038/s41589-025-01885-5.

References

1. Van Meer, G., Voelker, D. R. & Feigenson, G. W. Membrane lipids: where they are and how they behave. *Nat. Rev. Mol. Cell Biol.* **9**, 112–124 (2008).
2. Balla, T. Phosphoinositides: tiny lipids with giant impact on cell regulation. *Physiol. Rev.* **93**, 1019–1137 (2013).
3. Harayama, T. & Riezman, H. Understanding the diversity of membrane lipid composition. *Nat. Rev. Mol. Cell Biol.* **19**, 281–296 (2018).
4. Carman, G. M. & Han, G. S. Regulation of phospholipid synthesis in the yeast *Saccharomyces cerevisiae*. *Annu. Rev. Biochem.* **80**, 859–883 (2011).
5. Henry, S. A., Kohlwein, S. D. & Carman, G. M. Metabolism and regulation of glycerolipids in the yeast *Saccharomyces cerevisiae*. *Genetics* **190**, 317–349 (2012).
6. Zhang, Y. M. & Rock, C. O. Membrane lipid homeostasis in bacteria. *Nat. Rev. Microbiol.* **6**, 222–233 (2008).
7. Janmey, P. A. & Kinnunen, P. K. Biophysical properties of lipids and dynamic membranes. *Trends Cell Biol.* **16**, 538–546 (2006).
8. Di Paolo, G. & De Camilli, P. Phosphoinositides in cell regulation and membrane dynamics. *Nature* **443**, 651–657 (2006).
9. Kutateladze, T. G. Translation of the phosphoinositide code by PI effectors. *Nat. Chem. Biol.* **6**, 507–513 (2010).
10. Vítová, M. et al. The biosynthesis of phospholipids is linked to the cell cycle in a model eukaryote. *Biochim. Biophys. Acta Mol. Cell. Biol. Lipids* **1866**, 158965 (2021).
11. Atilla-Gokcumen, G. E. et al. Dividing cells regulate their lipid composition and localization. *Cell* **156**, 428–439 (2014).
12. Takhaveev, V. et al. Temporal segregation of biosynthetic processes is responsible for metabolic oscillations during the budding yeast cell cycle. *Nat. Metab.* **5**, 294–313 (2023).
13. Blank, H. M. et al. Abundances of transcripts, proteins, and metabolites in the cell cycle of budding yeast reveal coordinate control of lipid metabolism. *Mol. Biol. Cell* **31**, 1069–1084 (2020).

14. Ye, C., Sutter, B. M., Wang, Y., Kuang, Z. & Tu, B. P. A metabolic function for phospholipid and histone methylation. *Mol. Cell* **66**, 180–193.e188 (2017).
15. Zhu, Y. et al. Phospholipid biosynthesis modulates nucleotide metabolism and reductive capacity. *Nat. Chem. Biol.* **21**, 35–46 (2025).
16. Villasmil, M. L., Gallo-Ebert, C., Liu, H. Y., Francisco, J. & Nickels, J. T. Jr. A link between very long chain fatty acid elongation and mating-specific yeast cell cycle arrest. *Cell Cycle* **16**, 2192–2203 (2017).
17. Köberlin, M. S. et al. A fast-acting lipid checkpoint in G1 prevents mitotic defects. *Nat. Commun.* **15**, 2441 (2024).
18. Blank, H. M., Griffith, W. P. & Polymenis, M. Targeting APEX2 to the mRNA encoding fatty acid synthase β in yeast identifies interacting proteins that control its abundance in the cell cycle. *Mol. Biol. Cell* **34**, br20 (2023).
19. Blank, H. M. et al. Translational control of lipogenic enzymes in the cell cycle of synchronous, growing yeast cells. *EMBO J.* **36**, 487–502 (2017).
20. Maitra, N., Hammer, S., Kjerfve, C., Bankaitis, V. A. & Polymenis, M. Translational control of lipogenesis links protein synthesis and phosphoinositide signaling with nuclear division in *Saccharomyces cerevisiae*. *Genetics* **220**, iyab171 (2022).
21. Tu, B. P., Kudlicki, A., Rowicka, M. & McKnight, S. L. Logic of the yeast metabolic cycle: temporal compartmentalization of cellular processes. *Science* **310**, 1152–1158 (2005).
22. Cai, L., Sutter, B. M., Li, B. & Tu, B. P. Acetyl-CoA induces cell growth and proliferation by promoting the acetylation of histones at growth genes. *Mol. Cell* **42**, 426–437 (2011).
23. Papagiannakis, A., Niebel, B., Wit, E. C. & Heinemann, M. Autonomous metabolic oscillations robustly gate the early and late cell cycle. *Mol. Cell* **65**, 285–295 (2017).
24. Cheng, A. et al. A mitotic NADPH upsurge promotes chromosome segregation and tumour progression in aneuploid cancer cells. *Nat. Metab.* **5**, 1141–1158 (2023).
25. Slavov, N. & Botstein, D. Coupling among growth rate response, metabolic cycle, and cell division cycle in yeast. *Mol. Biol. Cell* **22**, 1997–2009 (2011).
26. Tu, B. P. & McKnight, S. L. Metabolic cycles as an underlying basis of biological oscillations. *Nat. Rev. Mol. Cell Biol.* **7**, 696–701 (2006).
27. Von Meyenburg, H. K. Energetics of the budding cycle of *Saccharomyces cerevisiae* during glucose limited aerobic growth. *Arch. Mikrobiol.* **66**, 289–303 (1969).
28. Murray, D. B., Beckmann, M. & Kitano, H. Regulation of yeast oscillatory dynamics. *Proc. Natl Acad. Sci. USA* **104**, 2241–2246 (2007).
29. Murray, D. B., Roller, S., Kuriyama, H. & Lloyd, D. Clock control of ultradian respiratory oscillation found during yeast continuous culture. *J. Bacteriol.* **183**, 7253–7259 (2001).
30. Klevecz, R. R., Bolen, J., Forrest, G. & Murray, D. B. A genomewide oscillation in transcription gates DNA replication and cell cycle. *Proc. Natl Acad. Sci. USA* **101**, 1200–1205 (2004).
31. Kuang, Z. et al. High-temporal-resolution view of transcription and chromatin states across distinct metabolic states in budding yeast. *Nat. Struct. Mol. Biol.* **21**, 854–863 (2014).
32. Mellor, J. The molecular basis of metabolic cycles and their relationship to circadian rhythms. *Nat. Struct. Mol. Biol.* **23**, 1035–1044 (2016).
33. Wang, G. Z. et al. Cycling transcriptional networks optimize energy utilization on a genome scale. *Cell Rep.* **13**, 1868–1880 (2015).
34. Murray, D. B., Klevecz, R. R. & Lloyd, D. Generation and maintenance of synchrony in *Saccharomyces cerevisiae* continuous culture. *Exp. Cell. Res.* **287**, 10–15 (2003).
35. Tu, B. P. et al. Cyclic changes in metabolic state during the life of a yeast cell. *Proc. Natl Acad. Sci. USA* **104**, 16886–16891 (2007).
36. Yang, S., Xue, J. & Ye, C. Protocol for rapid and accurate quantification of phospholipids in yeast and mammalian systems using LC–MS. *STAR Protoc.* **3**, 101769 (2022).
37. Bier, M., Bakker, B. M. & Westerhoff, H. V. How yeast cells synchronize their glycolytic oscillations: a perturbation analytic treatment. *Biophys. J.* **78**, 1087–1093 (2000).
38. Tilcock, C. P., Cullis, P. R., Hope, M. J. & Gruner, S. M. Polymorphic phase behavior of unsaturated lysophosphatidylethanolamines: a 31P NMR and X-ray diffraction study. *Biochemistry* **25**, 816–822 (1986).
39. Hsieh, W. C. et al. Glucose starvation induces a switch in the histone acetylome for activation of gluconeogenic and fat metabolism genes. *Mol. Cell* **82**, 60–74 (2022).
40. McMaster, C. R. & Bell, R. M. Phosphatidylcholine biosynthesis in *Saccharomyces cerevisiae*. Regulatory insights from studies employing null and chimeric sn-1,2-diacylglycerol choline- and ethanolaminephosphotransferases. *J. Biol. Chem.* **269**, 28010–28016 (1994).
41. Loewen, C. J. et al. Phospholipid metabolism regulated by a transcription factor sensing phosphatidic acid. *Science* **304**, 1644–1647 (2004).
42. Hofbauer, H. F. et al. The molecular recognition of phosphatidic acid by an amphipathic helix in Opi1. *J. Cell Biol.* **217**, 3109–3126 (2018).
43. Ortega-Arzola, E., Higgins, P. M. & Cockell, C. S. The minimum energy required to build a cell. *Sci. Rep.* **14**, 5267 (2024).
44. Casanovas, A. et al. Quantitative analysis of proteome and lipidome dynamics reveals functional regulation of global lipid metabolism. *Chem. Biol.* **22**, 412–425 (2015).
45. Ernst, R., Ballweg, S. & Levental, I. Cellular mechanisms of physicochemical membrane homeostasis. *Curr. Opin. Cell Biol.* **53**, 44–51 (2018).
46. Bloom, M., Evans, E. & Mouritsen, O. G. Physical properties of the fluid lipid-bilayer component of cell membranes: a perspective. *Q. Rev. Biophys.* **24**, 293–397 (1991).
47. Bagatolli, L. A., Ipsen, J. H., Simonsen, A. C. & Mouritsen, O. G. An outlook on organization of lipids in membranes: searching for a realistic connection with the organization of biological membranes. *Prog. Lipid Res.* **49**, 378–389 (2010).
48. Renne, M. F. & de Kroon, A. The role of phospholipid molecular species in determining the physical properties of yeast membranes. *FEBS Lett.* **592**, 1330–1345 (2018).
49. Baumgart, T., Capraro, B. R., Zhu, C. & Das, S. L. Thermodynamics and mechanics of membrane curvature generation and sensing by proteins and lipids. *Annu. Rev. Phys. Chem.* **62**, 483–506 (2011).
50. Boumann, H. A., Chin, P. T., Heck, A. J., De Kruijff, B. & De Kroon, A. I. The yeast phospholipid N-methyltransferases catalyzing the synthesis of phosphatidylcholine preferentially convert di-C16:1 substrates both in vivo and in vitro. *J. Biol. Chem.* **279**, 40314–40319 (2004).
51. Boumann, H. A. et al. The two biosynthetic routes leading to phosphatidylcholine in yeast produce different sets of molecular species. Evidence for lipid remodeling. *Biochemistry* **42**, 3054–3059 (2003).
52. Schink, K. O., Tan, K. W. & Stenmark, H. Phosphoinositides in Control of Membrane Dynamics. *Annu. Rev. Cell Dev. Biol.* **32**, 143–171 (2016).
53. Posor, Y., Jang, W. & Haucke, V. Phosphoinositides as membrane organizers. *Nat. Rev. Mol. Cell Biol.* **23**, 797–816 (2022).

54. Renne, M. F. et al. Molecular species selectivity of lipid transport creates a mitochondrial sink for di-unsaturated phospholipids. *EMBO J.* **41**, e106837 (2022).
55. Bürgermeister, M., Birner-Grünberger, R., Heyn, M. & Daum, G. Contribution of different biosynthetic pathways to species selectivity of aminoglycerophospholipids assembled into mitochondrial membranes of the yeast *Saccharomyces cerevisiae*. *Biochim. Biophys. Acta* **1686**, 148–160 (2004).
56. Carman, G. M. & Henry, S. A. Phospholipid biosynthesis in the yeast *Saccharomyces cerevisiae* and interrelationship with other metabolic processes. *Prog. Lipid Res.* **38**, 361–399 (1999).

Methods

Yeast strains and media

The prototrophic, haploid CEN.PK strain background was used in this investigation[57]. Gene deletions and the creation of carboxy-terminal tags in this background were carried out through conventional PCR-based methods, using resistance cassettes with appropriate flanking sequences and employing homologous recombination for integration at their native locus. All transformations were performed using the lithium acetate method. Strains and genetic alterations were verified through PCR, sequencing and phenotype analysis. Specifically, the depletion of lipid droplets in *pah1Δ* and *dga1Δlro1Δ* mutants was confirmed via microscopy after BODIPY staining. To generate the *opi1*^{Y127D} mutant, we introduced the point mutation to the *OPI1*-containing pFA6 plasmid using primers with the desired mutation that amplifies the entire plasmid template using the 2× MultiF Seamless Assembly Mix kit (ABclonal). The DNA fragment was then amplified by PCR and transformed into the *opi1Δ* mutant through homologous recombination. The integration of the point mutation was confirmed through sequencing. The growth defect of *opi1*^{Y127D} mutant in media lacking inositol was confirmed[58]. To create the *psd1*^{GAPpr} mutant, we first constructed the HO plasmid containing GAP promoter-driven *PSD1* fragment via fusion PCR. The DNA fragment amplified by PCR was transformed into WT cells. The integration of the GAP promoter to the chromosomal loci of *PSD1* was confirmed through sequencing. The information on strains, primers and plasmids is provided in Supplementary Data 5.

The following media were used in this study: yeast extract peptone dextrose (YPD) medium was composed of 2% yeast extract, 2% peptone and 2% glucose. YPD medium was used to cultivate yeast cells overnight from a single colony on a solid plate before conducting the YMC experiments. Synthetic defined (SD) medium was composed of 0.17% yeast nitrogen base without amino acids, including 0.5% ammonium sulfate (Difco) and 2% glucose. SD medium was used in tracing experiments, wherein unlabeled glucose in SD was substituted by [U−^{13}C6] glucose to create ^{13}C-tracing medium. YMC medium for continuous culture was composed of 0.5% ammonium sulfate, 0.2% potassium dihydrogen phosphate, 0.05% magnesium sulfate heptahydrate, 0.08% calcium chloride, 0.0018% iron sulfate heptahydrate, 0.0009% zine sulfate heptahydrate, 0.0005% copper sulfate, 0.00008% manganese chloride tetrahydrate, 0.1% yeast extract, 1% glucose, 0.035% (vol/vol) sulfuric acid and 0.05% Antifoam 204.

Continuous culture conditions for the YMC

The bioreactor (INFORS, Minifors2 3.0 l) was used to establish continuous culture conditions for the YMC. Each run involved setting the bioreactor to a temperature of 30 °C, a pH of 3.4, agitation at 1,000 rpm and aeration at 1 l min^{-1}, with a working volume of 1 l. Once the system reached equilibrium, each YMC was initiated by inoculating 10 OD_{600} units of cells cultured overnight in YPD medium. Following growth saturation, the yeast cells were subjected to a minimum of 12 h of starvation. After this starvation period, fresh YMC medium containing 1% glucose was continuously infused at a dilution rate of 0.1 per h. Robust YMC cycles in oxygen consumption were observed in WT, *opi1Δ* and *cpt1Δept1Δ* cells. However, WT cells failed to sustain the YMC in the presence of 1 mM exogenous choline. The *cho2Δopi3Δ* mutant was unable to undergo metabolic cycles even with choline supplementation. Conversely, the *ino1Δ* mutant displayed metabolic cycles with supplementation of 1 mM inositol. Interestingly, the *psd1Δ* mutant was unable to undergo metabolic cycles but showed abnormal metabolic cycles with exogenous ethanolamine.

YMC sampling

Approximately 8 OD_{600} units of YMC cells per time interval were harvested from the bioreactor, snap-frozen using liquid nitrogen and stored at −80 °C. Specific time points for YMC sampling were indicated in the figures. The first time interval of a cycle was typically chosen to be at the RC phase, minimizing disruptions to the abrupt burst of oxygen consumption in the OX phase. For the mutant with aberrant cycling times, such as *psd1*^{GAPpr}, samples were collected after continuous feeding at the same phases as those of the WT cells.

Lipid extraction

Lipid extraction was carried out when all cycling samples were collected. Yeast lipids were extracted with chloroform/methanol (2:1; vol/vol) as described previously[36]. Cell pellets were resuspended in 0.5 ml mass spectrometry (MS)-grade methanol containing the spike-in standards (PC = 17:0, 1.97 μM; PE = 17:0, 2.08 μM and PS = 14:0, 2.14 μM) and lysed by bead-beating. Cell pellets and lysates were then transferred to glass tubes. Chloroform and citric acid were added to achieve phase separation. The bottom lipid phase was collected and dried using a vacuum concentrator system (Labconco).

Quantitative analysis of phospholipids using LC–MS

The dried lipid extracts were dissolved in a mixed MS-grade solution containing isopropanol, acetonitrile and water in the ratio of 2:1:1. Quality control (QC) samples were generated by combining equal volumes of each sample in the experiment. Lipidomix (Avanti) was added as an internal standard for the estimation of phospholipid concentrations. For quantitative analysis of phospholipids, 5 μl of samples was injected, with two QC samples were injected for every ten samples. Chromatographic separation of phospholipids was performed on a C18 column (ACQUITY UPLC BEH C18 column, 130 Å, 1.7 μM, 2.1 mm × 50 mm), followed by detection using multiple reaction monitoring (MRM) transitions of MS in negative ion mode (the QTRAP 6500+ System, AB SCIEX). This method had been previously optimized for the simultaneous detection of a library of yeast phospholipids (Supplementary Data 6). Liquid chromatography was configured as follows: buffer A—33.3% acetonitrile, 33.3% methanol, 33.4% water and 5 mM ammonium acetate; buffer B—100% isopropanol containing 5 mM ammonium acetate. Flow rate was 0.15 ml min^{-1} using the following gradient: 20% buffer B at T = 0 min, 20% buffer B at T = 1 min, 60% buffer B at T = 3 min, 98% buffer B at T = 20 min, 20% buffer B at T = 20.1 min and 20% buffer B at T = 25 min. The retention time for each MRM peak was compared to an appropriate standard. The area under each peak was then quantified using Analyst software OS v1.7.

Quantitative analysis of TAG using LC–MS

For quantitative analysis of TAG levels, lipid extracts were resuspended in an MS-grade solution containing a 1:1 mixture of methanol and methylene chloride, supplemented with 5 mM ammonium acetate, and Lipidomix as an internal standard. Each sample was injected with 5 μl, and two QC samples were injected for every ten samples to ensure consistency and reliability. Chromatographic separation of TAGs was achieved using a C18 column (ACQUITY UPLC BEH C18 column, 130 Å, 1.7 μM, 2.1 mm × 50 mm), followed by detection using MRM transitions of MS in positive ion mode (the QTRAP 6500+ System, AB SCIEX). Liquid chromatography was configured with buffer A consisting of 33.3% acetonitrile, 33.3% methanol, 33.4% water and 5 mM ammonium acetate, while buffer B comprised 100% isopropanol containing 5 mM ammonium acetate. Flow rate was set at 0.15 ml min^{-1}, using the following specified gradient: 20% buffer B at T = 0 min, 20% buffer B at T = 1 min, 60% buffer B at T = 3 min, 98% buffer B at T = 13 min, 20% buffer B at T = 13.1 min and maintained at 20% buffer until T = 20 min.

Lipid data processing and quantification

For phospholipid analysis, we employed a combined approach using both a home-made spike-in standard mixture and commercial lipidomix standards. The spike-in standards (PC = 17:0, 1.97 μM; PE = 17:0, 2.08 μM and PS = 14:0, 2.14 μM) were added directly to each sample during the extraction process. These standards served to monitor potential sample loss during extraction, ensuring accurate quantification of

phospholipid levels across all samples. It is important to note that no corrections were applied based on spike-in standard recovery in this study, as consistent recovery of the major phospholipid spike-in standards was observed across all samples. Lipidomix standards (Avanti Polar Lipids, 330707), which contain deuterated lipids, were added after extraction during the reconstitution process before LC–MS/MS analysis. While the use of the home-made spike-in standard mixture during extraction is a more cost-effective option, the commercial Lipidomix standards, containing a wider range of lipids with defined concentrations, provide more consistent and precise quantification across different lipid classes. To ensure accurate peak annotation for the detected lipids, phospholipid species at specific MRM transitions and elution times were verified using yeast mutants. The area under each peak was quantified using Analyst software and reinspected for accuracy to minimize potential errors. For TAG analysis, lipid extracts were resuspended in an MS-grade solution containing a 1:1 mixture of methanol and methylene chloride, supplemented with 5 mM ammonium acetate, which proved more efficient for dissolving TAG.

The molar concentration of a phospholipid species or TAG species in a sample (C_s) was calculated using the following equation:

$$C_s = C_{\text{std}} \times \frac{A_s}{A_{\text{std}}} \quad (1)$$

where C_s is the molar concentration of the target lipid species, C_{std} is the molar concentration of the corresponding deuterated internal standard, A_s is the measured LC–MS peak area (signal intensity) of the lipid species in the sample and A_{std} is the measured LC–MS peak area (signal intensity) of the internal standard.

The concentrations of different phospholipid species were subsequently normalized to the total phospholipid content to obtain the relative abundance of each species as a percentage. Additionally, class compositions were calculated as mol% to provide insights into the relative abundance of different phospholipid classes within the YMC. In some cases, the structural characteristics, such as the number of carbons or double bonds in the acyl chains of specific phospholipid classes, were analyzed to gain an understanding of the impact of lipid acyl composition.

Metabolic rate calculation

Metabolic rates were determined as follows: (1) determine the change in lipid concentration over time by calculating the difference in lipid concentration ($C(t_{n+1}) - C(t_n)$) between consecutive time points (t_{n+1} and t_n) × $C(t_{n+1})$ and $C(t_n)$ represent the absolute concentrations of the lipid at time points t_{n+1} and t_n, respectively, expressed in µM. (2) Calculate the metabolic rate by dividing the change in lipid concentration by the time interval between the two time points. This provides the rate of lipid synthesis (for increasing concentrations) or consumption (for decreasing concentrations) over the given time period.

Overall, metabolic rates are calculated using the following formula:

$$\text{Metabolic rate}\left(\frac{\text{nmol}}{\text{min}}\right) = \frac{C(t_{n+1}) - C(t_n)}{t_{n+1} - t_n} \times V \times 10^3 \quad (2)$$

where $C(t_{n+1})$ and $C(t_n)$ represent the absolute concentrations of the metabolite at consecutive time points t_{n+1} and t_n, expressed in µM (µmol l^{-1}), and V is the reaction volume in liters.

Curve fitting

The mol% data representing relative phospholipid abundances across two consecutive cycles of the YMC were subjected to curve fitting using a sine function:

$$f(x) = A \times \sin(2\pi \times (x + C)) \quad (3)$$

This analysis and visualization were conducted using RStudio (version 2021.90.351). The goodness-of-fit and statistical significance of the curve fitting were assessed using the coefficient of determination (R^2) and the P value, respectively. The frequency of this sinusoidal function represents the number of budding cycles per unit time (x). The maximum displacement is denoted by the amplitude (A), which indicates the relative change from the equilibrium position. The peak-to-peak amplitude ($2A$) represents the maximum fluctuation in phospholipid abundance and is determined by the maximal difference between synthesis and consumption. T_{trough} corresponds to the phase when phospholipid abundance is at its lowest point. C corresponds to a phase shift, which characterizes the temporal oscillation of a phospholipid species or class as a function of the YMC.

Fluorescence microscopy

For live cell imaging, WT cells with Opi1 chromosomally GFP-tagged at the C terminus were taken from the indicated times for imaging across the YMC. All images were taken under a ×100/1.4-NA oil-immersion objective lens with a Deltavision Elite microscope (Applied Precision, GE Healthcare).

RNA extraction and real-time qPCR analysis

RNA isolation of yeast cells under different growth conditions was carried out following the manufacturer's instructions using the MasterPure yeast RNA purification kit (Epicenter). RNA concentration was determined by absorbance at 260 nm. One microgram of RNA was reverse transcribed to cDNA using the HiScript III First Strand cDNA Synthesis Kit (Vazyme). Real-time PCR was performed in triplicate with the ChamQ SYBR qPCR Master Mix from Vazyme. Transcript levels of genes were normalized to *ACT1*.

Growth competition in the YMC

WT and *opi1Δ* cells precultured overnight in YPD were inoculated into the bioreactor system at the same density equivalent to 10 OD_{600} units. Every 12 h, the mixture growth was sampled by spreading cells onto the YPD plate, allowing the formation of single colonies. These YPD plates were then replicated onto YPD plates containing G418 to distinguish between WT and *opi1Δ* cells. The proportions of WT and *opi1Δ* cells at each indicated time point were determined by calculating the fraction of single colonies corresponding to each strain.

Determination of phospholipid and TAG turnover using [U–^{13}C6] glucose

In WT cells undergoing stable metabolic cycles, we performed substitution experiments by replacing the feeding YMC medium with a medium containing 1% [U–^{13}C6] glucose at the indicated phase. Samples were collected before the substitution and at the 20-min intervals thereafter. Following sample collection, lipid extraction was performed to quantify the remaining levels of each phospholipid and TAG species. The turnover rates for the abundances of phospholipid classes and TAG were calculated as a fraction relative to those before the substitution of the ^{13}C feeding medium. Specifically, samples taken within the first 100 min and those collected between 100 and 200 min were grouped to estimate average turnover rates. However, due to the slow dilution of ^{12}C by ^{13}C derived from [U–^{13}C6] glucose after substituting the medium containing 1% [U–^{13}C6] glucose in the YMC, the amounts of glycerolipids in the ^{13}C fully labeled form were not detectable. This poses a challenge to estimate the synthesis rate of phospholipids under YMC conditions.

Reverse stable isotope labeling to quantify the turnover and synthesis of phospholipids and TAG

To address the slow replacement of isotopic metabolites, we implemented a medium switch in the batch culture. WT and *pah1Δ* cells were precultured overnight in SD medium containing only [U–^{13}C6] glucose

and diluted to 0.2 OD_{600} with the same [U–^{13}C6] glucose SD medium to ensure full ^{13}C labeling. Following synchronization by growth saturation in [U–^{13}C6] glucose medium, the cells were harvested, washed and rediluted to 0.5 OD_{600} with SD medium containing nonlabeled glucose. At various time points, including one or two rounds of doubling when the OD_{600} reached 1.0 and 2.0, respectively, 4 OD_{600} units of cells were collected for lipid extraction. We quantified ^{13}C-labeled and unlabeled phospholipid and TAG species using specific MRM transitions. Specifically, we accounted for the mass shift resulting from the labeling changes in polar head groups, fatty acyl chains and the glycerol backbone, as illustrated in Extended Data Fig. 3c.

Statistical analysis

Normalized glycerolipid abundances were log-transformed, median-centered and clustered using the Spearman rank correlation algorithm with Cluster 3. Heatmaps were generated using Treeview 1.2.0. Sankey diagrams were created using Sankey MATIC, a web-based platform for visualizing flow diagrams. Statistical significance was determined by unpaired Student's *t* test (one-sided, except for sine wave fitting, which used a two-sided *t* test). *P* values and sample sizes (*n*) are provided in the figure legends.

Reporting summary

Further information on research design is available in the Nature Portfolio Reporting Summary linked to this article.

Data availability

All data supporting the findings of this study presented in this article are available within the article, Supplementary Information and source data. Source data are provided with this paper.

References

57. Van Dijken, J. P. et al. An interlaboratory comparison of physiological and genetic properties of four *Saccharomyces cerevisiae* strains. *Enzym. Microb. Technol.* **26**, 706–714 (2000).
58. Haider, A. et al. PCYT1A regulates phosphatidylcholine homeostasis from the inner nuclear membrane in response to membrane stored curvature elastic stress. *Dev. Cell* **45**, 481–495 (2018).

Acknowledgements

We thank the technical support from the Core Facility of Life Sciences Institute, Zhejiang University. This work was supported by grants from the National Key Research and Development Program of China (2023YFA1801100 and 2024YFA1803000), the National Natural Science Foundation of China (32270816 and 92057102), Double Thousand Plan of Jiangxi Province (jxsq2023102239), the Fundamental Research Funds for the Central Universities (226-2024-00088), a research fund from Zhejiang Provincial Key Laboratory for Cancer Molecular Cell Biology, the startup fund from the Life Sciences Institute of Zhejiang University and the 1000 Talents Program for Young Scholars (to C.Y.) and the National Natural Science Foundation of China (32321002 to P.X.).

Author contributions

C.Y. conceptualized the project, acquired funding and administered the project. S.Y. and C.Y. guided methodology development. S.Y., Y.W., S.H. and T.Z. conducted the investigation. S.Y. and Y.W. visualized the project. C.Y. and C.J. supervised the project. P.X. and C.Y. wrote the manuscript. All authors read, edited and approved the manuscript.

Competing interests

The authors declare no competing interests.

Additional information

Extended data is available for this paper at https://doi.org/10.1038/s41589-025-01885-5.

Supplementary information The online version contains supplementary material available at https://doi.org/10.1038/s41589-025-01885-5.

Correspondence and requests for materials should be addressed to Cunqi Ye.

Peer review information *Nature Chemical Biology* thanks Rutilio Fratti, Mike Renne and the other, anonymous reviewer(s) for their contribution to the peer review of this work.

https://doi.org/10.1038/s41589-025-01885-5

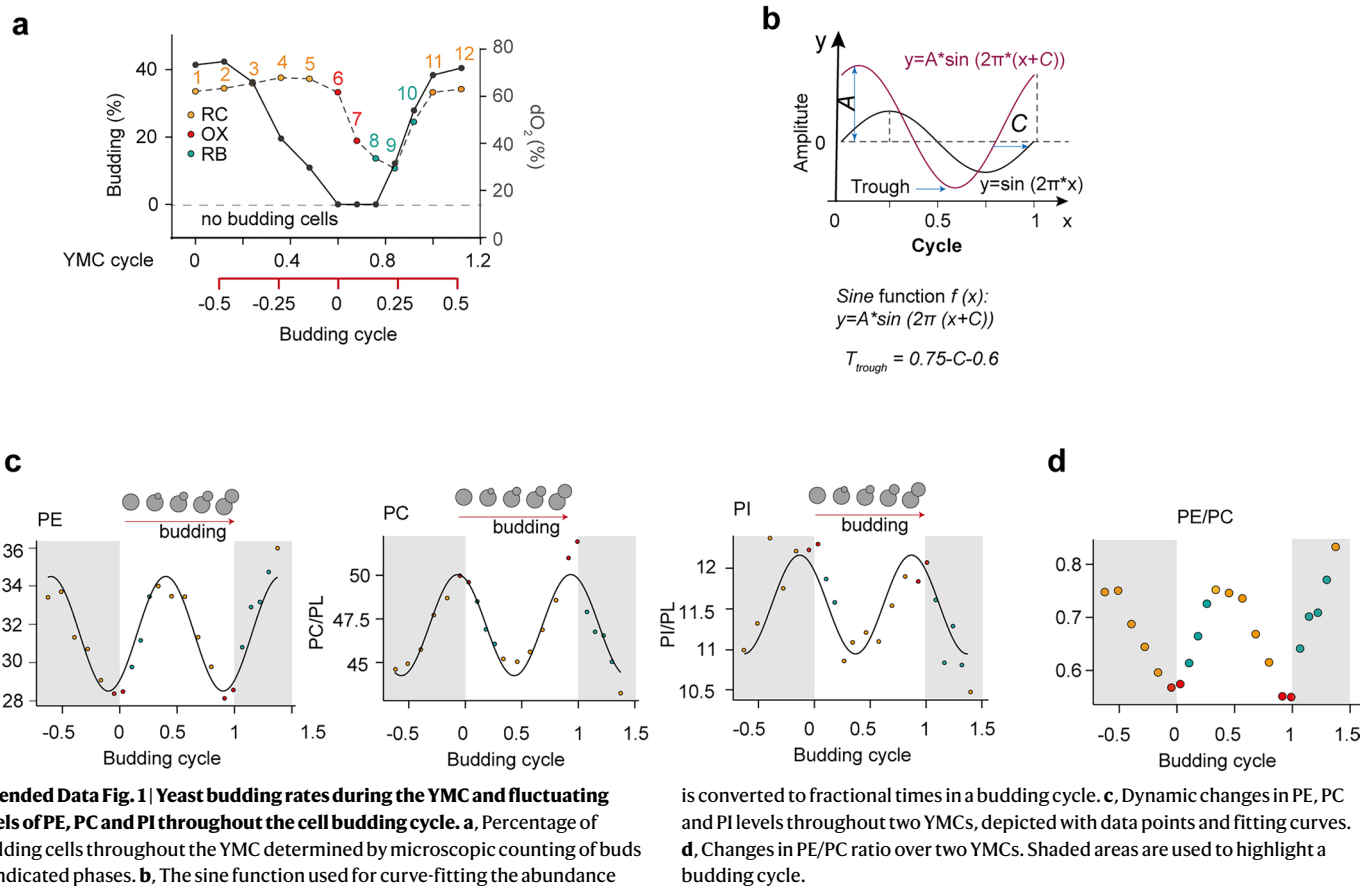

Extended Data Fig. 1 | Yeast budding rates during the YMC and fluctuating levels of PE, PC and PI throughout the cell budding cycle. a, Percentage of budding cells throughout the YMC determined by microscopic counting of buds at indicated phases. **b**, The sine function used for curve-fitting the abundance dynamics in phospholipids throughout two consecutive cycles of the YMC. T_{trough} is converted to fractional times in a budding cycle. **c**, Dynamic changes in PE, PC and PI levels throughout two YMCs, depicted with data points and fitting curves. **d**, Changes in PE/PC ratio over two YMCs. Shaded areas are used to highlight a budding cycle.

https://doi.org/10.1038/s41589-025-01885-5

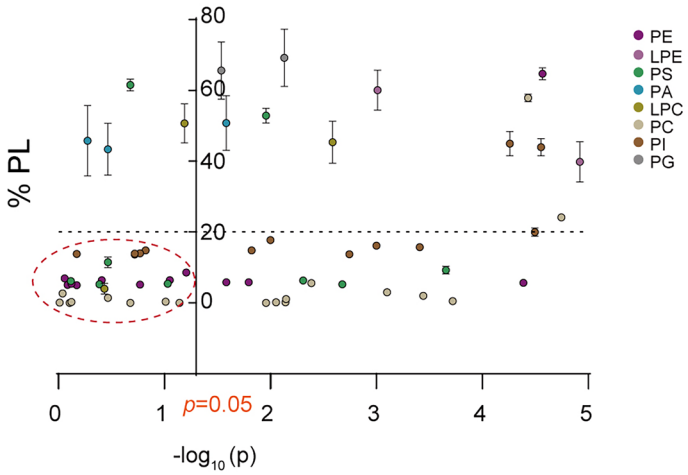

Extended Data Fig. 2 | Significant fitting exhibits a bias towards abundant phospholipids. Analysis of the correlation between species abundance and curve fitting significance. Data are represented as mean ± s.d. (n = 22 biologically independent samples).

https://doi.org/10.1038/s41589-025-01885-5

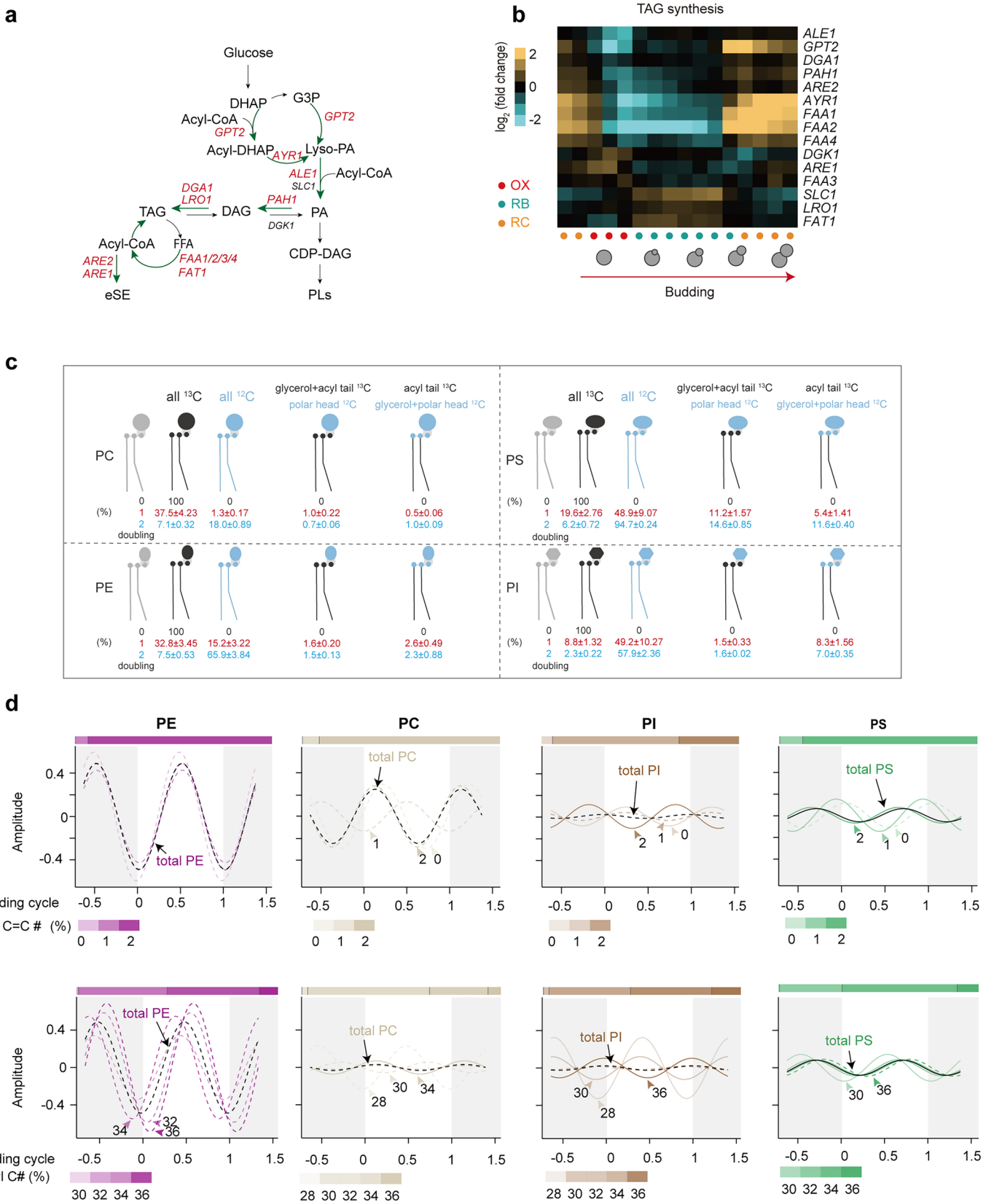

Extended Data Fig. 3 | RIL to quantify the turnover and synthesis of phospholipids. a, Schematic of the TAG biosynthesis pathway with genes at respective steps highlighted in red. **b**, Heatmap depicting the oscillatory expression of genes involved in TAG biosynthesis across the YMC. The heatmap is generated using RNA-seq data previously published[31]. **c**, Relative abundance of indicated phospholipid classes with acyl chains, polar head groups and the glycerol backbone individually or combinatorially labeled with ^{13}C and ^{12}C after two rounds of doubling in the RIL experiment. Relative abundance was calculated by normalizing to the total amount of corresponding lipid classes with full ^{13}C labeling before the RIL switch. **d**, Sine waves fitting of PE, PC, PI and PS abundance in the *dga1Δlro1Δ* mutant of the YMC, characterized by their acyl composition. Solid lines indicate fitting of statistical significance ($P < 0.05$), while dashed lines represent nonsignificant fitting. Statistical analyses were performed using a two-sided *t*-test in **d**. Shaded areas are used to highlight a budding cycle.

https://doi.org/10.1038/s41589-025-01885-5

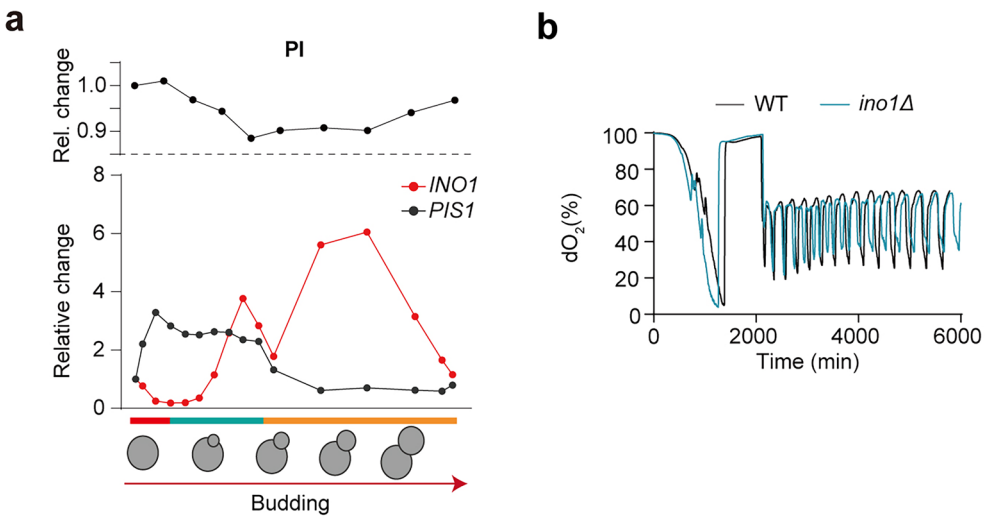

Extended Data Fig. 4 | Oscillation in PI abundance and transcripts of genes involved in PI biosynthesis. a, Temporal oscillations in the abundance of PI and the transcript levels of PI biosynthetic genes within a budding cycle. **b**, Oxygen consumption curves of WT and *ino1Δ* mutants with 1 mM myo-inositol.

https://doi.org/10.1038/s41589-025-01885-5

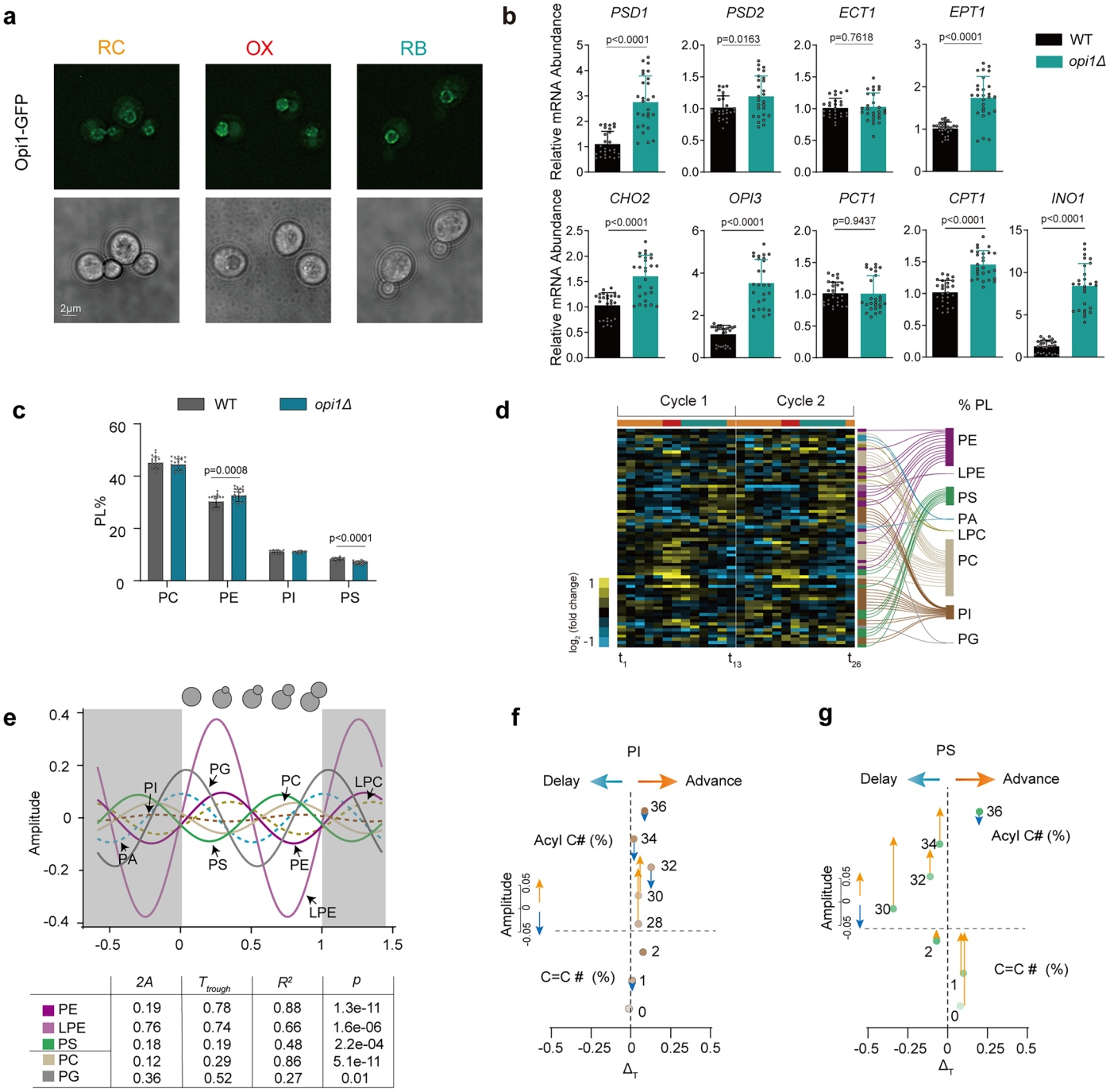

Extended Data Fig. 5 | Disruption of the Henry regulatory circuit shifts temporal oscillations in phospholipids. a, Representative Opi1–GFP fluorescence images at different YMC phases. Data shown are representative of two independent experiments with similar results. **b**, Relative mRNA levels of phospholipid biosynthesis genes in WT and *opi1Δ* cells during the YMC. Data are presented as mean ± s.d. ($n = 27$ biologically independent samples). **c**, PE, PC, PI and PS abundance (% PL) in WT ($n = 22$ biologically independent samples) and *opi1Δ* cells ($n = 26$ biologically independent samples) across the YMC. Data are presented as mean ± s.d. **d**, Hierarchical clustering of phospholipids in *opi1Δ* cells across the YMC. Data normalized to total ion counts, log-transformed and clustered (Spearman rank). Sankey diagram shows phospholipid class distribution. **e**, Top, sine waves representing major phospholipid classes in the *opi1Δ* mutant. Solid lines indicate fitting of statistical significance ($P < 0.05$), while dashed lines represent nonsignificant fitting. Bottom, summary table of fitting parameters. Shaded areas are used to highlight a budding cycle. **f**,**g**, Comparison of PI (**f**) and PS (**g**) oscillations between WT and the *opi1Δ* mutant, showing differences in T_{trough} and amplitude across their molecular species. Statistical analyses were performed using an unpaired *t* test in **b** and **c**. Statistical analyses were performed using a two-sided *t* test in **e**. Shaded areas are used to highlight a budding cycle.

nature portfolio

Corresponding author(s): Cunqi Ye

Last updated by author(s): Feb 21, 2025

Reporting Summary

Nature Portfolio wishes to improve the reproducibility of the work that we publish. This form provides structure for consistency and transparency in reporting. For further information on Nature Portfolio policies, see our Editorial Policies and the Editorial Policy Checklist.

Statistics

For all statistical analyses, confirm that the following items are present in the figure legend, table legend, main text, or Methods section.

n/a	Confirmed
☐	☒ The exact sample size (*n*) for each experimental group/condition, given as a discrete number and unit of measurement
☐	☒ A statement on whether measurements were taken from distinct samples or whether the same sample was measured repeatedly
☐	☒ The statistical test(s) used AND whether they are one- or two-sided *Only common tests should be described solely by name; describe more complex techniques in the Methods section.*
☒	☐ A description of all covariates tested
☒	☐ A description of any assumptions or corrections, such as tests of normality and adjustment for multiple comparisons
☐	☒ A full description of the statistical parameters including central tendency (e.g. means) or other basic estimates (e.g. regression coefficient) AND variation (e.g. standard deviation) or associated estimates of uncertainty (e.g. confidence intervals)
☐	☒ For null hypothesis testing, the test statistic (e.g. *F*, *t*, *r*) with confidence intervals, effect sizes, degrees of freedom and *P* value noted *Give P values as exact values whenever suitable.*
☒	☐ For Bayesian analysis, information on the choice of priors and Markov chain Monte Carlo settings
☒	☐ For hierarchical and complex designs, identification of the appropriate level for tests and full reporting of outcomes
☒	☐ Estimates of effect sizes (e.g. Cohen's *d*, Pearson's *r*), indicating how they were calculated

Our web collection on statistics for biologists contains articles on many of the points above.

Software and code

Policy information about availability of computer code

Data collection	Intracellular metabolites were measured using the QTRAP 6500+ System, ABSCIEX. The raw data were extracted with the software Analyst v1.7.2 and OS v1.7 from SCIEX. Real-time PCR was performed in a Bio-Rad CFX96 Connect device. All images were taken under a 100x,1.4 NA oil-immersion objective lens with a Deltavision Elite microscope (Applied Precision, GE). Curve fitting analysis and visualization were conducted using RStudio (version 2021.90.351).
Data analysis	The normalized abundances of metabolites were log-transformed, centered about the median, and clustered by Spearman rank correlation algorithm using Cluster 3, and heat maps were obtained by the software Treeview 1.2.0. The fitting of the sine curve was completed using the R language, primarily involving the packages: data.table (1.14.8), tidyverse (1.3.1), readxl (1.4.2), pheatmap (1.0.12), dendextend (1.17.1), ggrepel (0.9.3), scales (1.2.0), and latex2exp.Sankey diagrams were created using Sankey MATIC, a web-based platform for visualizing flow diagrams.

For manuscripts utilizing custom algorithms or software that are central to the research but not yet described in published literature, software must be made available to editors and reviewers. We strongly encourage code deposition in a community repository (e.g. GitHub). See the Nature Portfolio guidelines for submitting code & software for further information.

Data

Policy information about availability of data

All manuscripts must include a data availability statement. This statement should provide the following information, where applicable:

- Accession codes, unique identifiers, or web links for publicly available datasets
- A description of any restrictions on data availability
- For clinical datasets or third party data, please ensure that the statement adheres to our policy

All data supporting the findings of this study presented in this article are available within the article, supplementary information, and source data. Source data are provided with this paper.

Human research participants

Policy information about studies involving human research participants and Sex and Gender in Research.

Reporting on sex and gender	N/A
Population characteristics	N/A
Recruitment	N/A
Ethics oversight	N/A

Note that full information on the approval of the study protocol must also be provided in the manuscript.

Field-specific reporting

Please select the one below that is the best fit for your research. If you are not sure, read the appropriate sections before making your selection.

☒ Life sciences ☐ Behavioural & social sciences ☐ Ecological, evolutionary & environmental sciences

For a reference copy of the document with all sections, see nature.com/documents/nr-reporting-summary-flat.pdf

Life sciences study design

All studies must disclose on these points even when the disclosure is negative.

Sample size	Sample size was chosen based on experimental variability and the requirement of experimental samples for statistical analysis. At least three biological replicates per group were collected to perform statistical testing, which is sufficient for a minimal data set underlying the figures provided in the paper in order to support and interpret our central findings. Detailed n is indicated in the figure legends. No statistical method was used to determine the sample size.
Data exclusions	No data or samples were excluded from the analysis.
Replication	Experiments were performed at least twice to make sure that the results are reproducible, and representative data are shown. All attempts at replication were successful. Details are shown in Method.
Randomization	All samples were randomly allocated to experimental groups and processed.
Blinding	For the analyses of the qPCR data and cellular metabolites, blinding was not necessary since these analyses were observer independent. Blinding was performed during the acqusition of the metabolic raw data. The researcher who inspected the spectra intensities were blinded to the sample information.

Reporting for specific materials, systems and methods

We require information from authors about some types of materials, experimental systems and methods used in many studies. Here, indicate whether each material, system or method listed is relevant to your study. If you are not sure if a list item applies to your research, read the appropriate section before selecting a response.

Materials & experimental systems

n/a	Involved in the study
☒	☐ Antibodies
☐	☒ Eukaryotic cell lines
☒	☐ Palaeontology and archaeology
☒	☐ Animals and other organisms
☒	☐ Clinical data
☒	☐ Dual use research of concern

Methods

n/a	Involved in the study
☒	☐ ChIP-seq
☒	☐ Flow cytometry
☒	☐ MRI-based neuroimaging

Eukaryotic cell lines

Policy information about cell lines and Sex and Gender in Research

Cell line source(s)	The prototrophic CEN.PK strain of the budding yeast S. cerevisiae background was used in all experiments.
Authentication	None of the cell lines used were authenticated.
Mycoplasma contamination	The yeast cells were not tested for mycoplasma.
Commonly misidentified lines (See ICLAC register)	No commonly misidentified cell lines were involved in this study.